5. Plasmon-Coupled Resonance Energy Transfer and Photocatalysis: Theory and Application

Yeonjun Jeong[1] *and George C. Schatz*[1,2*]

[1]Department of Chemistry and [2]Graduate Program in Applied Physics, Northwestern University, Evanston, Illinois 60208, United States

This Chapter describes two very active topics in the field of plasmonics: energy transfer and photocatalysis. In *plasmonic photocatalysis*, light in the visible or near-infrared interacts with Ag or Au (or other) nanoparticles (NPs), exciting collective excitations of the conduction electrons known as plasmons, and the plasmons subsequently dephase to give electron–hole pairs, and these then cause chemical reactions in molecules that are nearby the NPs. The Chapter provides a review of the current experiments and theory in this area, especially highlighting recent nonadiabatic dynamics studies that have simulated this process in real time for the photocatalytic dissociation of H_2 on a Au NP. In *plasmon-coupled resonance energy transfer* (PC-RET), electromagnetic (EM) energy transfers between a donor molecule and an acceptor molecule, with a nearby Ag or Au particle serving as a plasmonically excited intermediate to enhance the transfer rate. The Chapter reviews recent experimental literature in this area, and then it presents a comprehensive study of the theory of PC-RET, emphasizing the role of electrodynamics (ED), and including both the purely classical theory of energy transfer and theory based on Fermi's Golden rule.

Keywords: plasmonic photocatalysis, plasmon-coupled resonance energy transfer, Green's function, quasistatic

Biographies

Yeonjun Jeong is currently a Ph.D. student in Chemistry at Northwestern University. He received his B.S. Chemistry at Pohang University of Science and Technology (POSTECH) under the supervision of Professor Young Min Rhee. His research focuses on the theoretical study of plasmon-mediated energy transfer among molecules and plasmonic nanostructures.

George C. Schatz is the Morrison Professor of Chemistry at Northwestern University. He received his undergraduate degree at Clarkson University and Ph.D. at Caltech. He was a postdoc at MIT and has been at Northwestern since 1976.

Schatz is a theoretician specializing in electronic structure methods, dynamical processes, electrodynamics, and statistical mechanics, who studies the optical, structural and thermal properties of nanomaterials, including plasmonic nanoparticles, catalysts, DNA and peptide self-assembled nanostructures, and carbon-based materials, with applications to chemical and biological sensing, electronic and biological materials, heterogeneous catalysis and solar energy.

Contents

Abbreviations

4,4′-bipyridine (BPY)
trans-1,2-bis(4-pyridyl)ethylene (BPE)
Boundary element method (BEM)
Chemical mechanism (CM)
Classical electrodynamics (CED)
Density functional theory (DFT)
Discrete dipole approximation (DDA)
Donor–acceptor (D–A)
Electrodynamics (ED)
Electromagnetic (EM)
Finite-difference time-domain (FDTD)
Finite element method (FEM)
Indium tin oxide (ITO)
Kinetic isotope effect (KIE)
Modified long-wavelength approximation (MLWA)
Metal–organic framework (MOF)
Nanoparticle (NP)
Plasmon-coupled resonance energy transfer (PC-RET)
Quantum electrodynamics (QED)
Quantum mechanics (QM)
Rate-determining step (RDS)
Real-time (RT)
Resonance energy transfer (RET)
Time-dependent density functional theory (TDDFT)
Transmission electron microscopy (TEM)

5.1 Introduction

When light in the visible interacts with Ag or Au (and some other) nanoparticles (NPs), the conduction electrons are coherently excited as an oscillating charge cloud (Fig. 1a), a process known as plasmon excitation. This leads to the striking red color of colloidal gold, and yellow for silver, reflecting the extremely strong extinction (absorption plus scattering) that is associated with exciting plasmons. In the last fifty years, the plasmonic properties of colloidal NPs have transitioned from only being relevant to stained glass windows and other art objects, to being important in a wide variety of nanotechnology applications, including photocatalysis, medical

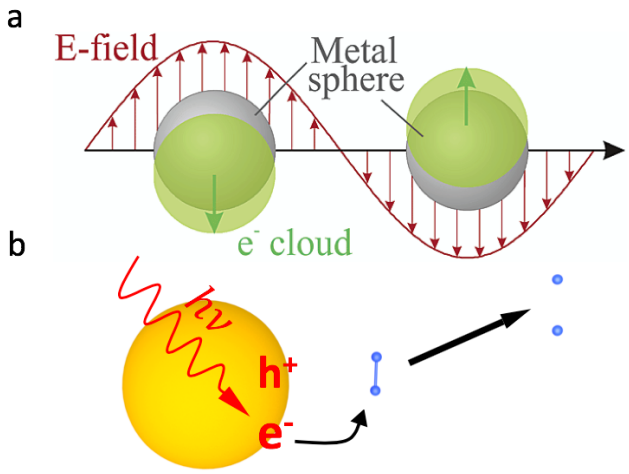

Fig. 1 Schematic descriptions of the driving force of plasmon-enhanced chemistry and plasmon-coupled resonance energy transfer: (**a**) generation of plasmons as electrons in the metal sphere oscillate under the external electric field, and (**b**) generation of hot charge carriers by an incident light, which leads to charge transfer to an adjacent molecule and further reactions. **a**, Reprinted from [1] © 2003 American Chemical Society; **b**, adapted from [2] © 2018 American Chemical Society

diagnostics and other sensing applications, therapeutics for destroying tumors, optoelectronic devices such as disk drive components, lasers, and solar energy materials. In this Chapter we focus on two specific applications of plasmonics that are often found in the same physical system: plasmon-enhanced chemistry and plasmon-coupled resonance energy transfer (PC-RET), both of which have advanced significantly in the last five years.

Plasmon-enhanced chemistry refers to the enhancement of chemical reactions due to proximity of the plasmonic particle to the molecule that undergoes reaction. There are two distinct mechanisms for this process: field enhanced chemistry and electron-induced chemistry. The field enhancement mechanism arises because the oscillating dipole (or higher multipole) moment that is induced in the metal particle when plasmon excitation occurs has a large electric field associated with it that interacts with a nearby molecule. This dipole field can be larger near to the NP than the field of the light that induced the dipole in the first place, so if the molecule can undergo a photoinduced reaction (by absorbing light to a reactive potential energy surface), the rate of this reaction will be higher. This is a passive process where the only role of the particle is to amplify the field experienced by the nearby molecule. The second mechanism involves the conversion of plasmon excitation into electrons or holes that are able to interact with molecules

near the particles (Fig. 1b), resulting in a photocatalytic chemical reaction, often with the molecule becoming an electronically excited transient ion. Both aspects of plasmon-enhanced chemistry have been reviewed in the past,[3] but especially the photocatalysis field has evolved rapidly, so our discussion in Sections 5.2 and 5.3 below will emphasize this.

Plasmon-coupled resonance energy transfer refers to the transfer of photoexcitation from a donor molecule to an acceptor molecule in the presence of a nearby plasmonic NP. This topic is related to donor–acceptor (D–A) energy transfer that is described by Förster theory, but when plasmonic particles participate in the process, the transfer can become much more efficient and long ranged.[94, 96-98, 100-109] When molecules are in immediate contact with metal NPs, their excited states are often quenched upon photoexcitation, and in some cases, electrons are transferred between molecule and particle, which is related to the plasmonic photocatalysis process discussed above. PC-RET typically becomes competitive with quenching when the molecules are separated by several nm from the NPs. In this limit, electron transfer is not important, and energy transfer can be dominant. However, it should be noted that there can also be plasmon-coupled molecular fluorescence, which competes with energy transfer. The branching between fluorescence and energy transfer is a complex function of D–A separation, as well as the distance of the molecules from the plasmonic NPs, so the details of these processes are only starting to be understood. These issues also highlight the interplay between plasmonic photocatalysis and PC-RET, such that it is appropriate to review both in this article. PC-RET is described in Sections 5.4 and 5.5 of this Chapter, including a brief review of representative experiments, and then a comprehensive discussion of the theory.

5.2 Plasmonic Photocatalysis: Experiments

5.2.1 Photocatalysis by Plasmonic Metals

Plasmon-enhanced photocatalysis is an active area of research in many laboratories, as has been reviewed,[4-14] with recent experimental reports in which Ag, Au or Al NPs have been involved in such processes as water oxidation,[15] H_2 dissociation,[16-18] propylene epoxidation,[19] and many others.[20, 21] There is also much interest (both experiment and theory) in using the hot electrons that are thought to be important in plasmon enhanced chemistry in hot-carrier solar cells and other devices.[9, 10, 22-29] And in the Van Duyne group at Northwestern, surface-enhanced Raman scattering (SERS) spectra have observed negative ions and other electron-driven photoproducts of the molecules 4,4′-bipyridine (BPY)[30] and trans-1,2-bis(4-pyridyl)ethylene (BPE)[31] after irradiation of Au NPs with 500 nm light, thus directly revealing the initial effects associated with plasmon driven electrons. It was shown that plasmon-enhanced chemistry can give different product selectivity compared to its thermal counterpart.[32, 33] Catalysis by hot electrons/holes generated from interband transitions on plasmonic metals by UV illumination is possible,[32, 34, 35] but we do not consider this type of reaction in this Chapter as it does not involve plasmons.

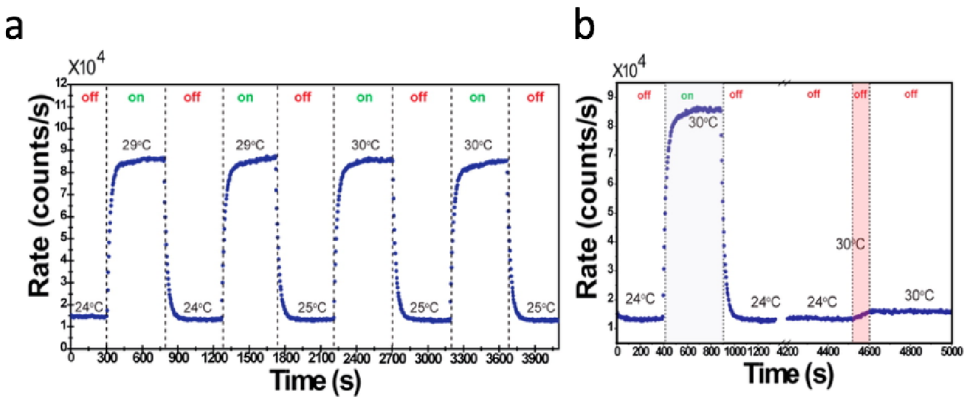

Fig. 2 (**a**) Rate of HD formation as a result of the reaction between H_2 and D_2 using 1.7 wt % Au/TiO2 photocatalyst measured versus time as light is turned on and off. Temperature of the system is labeled for each time block. (**b**) Without light, setting the temperature to that of when the light was on (depicted as a red block) had little effect on the reaction rate, confirming the photocatalysis of the system. Reprinted from [36] © 2013 American Chemical Society

A particularly simple and useful reaction to understand plasmonic photocatalysis involves H_2 dissociation near a Au NP as there are no side reactions. Halas and coworkers have shown (Fig. 2) that H_2 dissociation can be catalyzed at room temperature in the visible range, as flowing H_2 and D_2 through Au NPs supported by a TiO_2 substrate resulted in the generation of HD molecules.[36] When the light was on, the HD formation rate was increased by about an order of magnitude. Without light, setting the temperature to match that for the case when the light was on led to little increase of the reaction rate, confirming that the catalysis was a photon induced effect. In a subsequent paper,[17] the supporting matrix was changed to SiO_2 and the reaction rate was almost two orders of magnitude higher than the TiO_2 case. This is because SiO_2 has a much larger band gap than TiO_2 and thus thermally excited electrons cannot populate the conduction band of SiO_2. The conduction band of TiO_2 is located at a relatively low energy level, which facilitates draining of the hot electrons in the Au particles, reducing the catalytic activity.

Another important role of the oxide layer is as the 'dampener' of the kinetic energy of the H_2 molecule. The porous oxide layer has a higher accommodation coefficient for H_2 than the bare Au NP, and the H_2 molecules stay physisorbed for a longer time near the Au NPs. In the same research group, an Al–Pd nanodisk heterodimer was fabricated so that the strong absorption cross-section feature of Al and the catalytic character of Pd are combined.[18] Here, plasmons first generated in the Al disk force plasmon excitation in the Pd disk. Then hot electrons are generated and transferred to the anti-bonding orbital of the dihydrogen molecules, leading to dissociation. The influence of polarization angle, power of the incident light, wavelength, and the gap between the two disks was investigated.

Studies by Christopher, Xin, and Linic [37] provides a comprehensive view of the mechanism of plasmonic photocatalytic oxidation reactions through analyzing the O_2 dissociation step. In this work, Ag nanocubes were used to generate ethylene oxide from ethylene and O_2, and the O_2 dissociation step was postulated as the rate-determining step (RDS). The reactivity as a function of long-pass filter wavelength matched the plasmon intensity profile (calculated by multiplying the wavelength-dependent source intensity by the wavelength-dependent extinction spectrum and integrating over the wavelength to the filter cutoff wavelength), confirming that the reaction occurs through the photocatalytic mechanism (plasmons). The energy difference between O_2 and O_2^- on the Ag

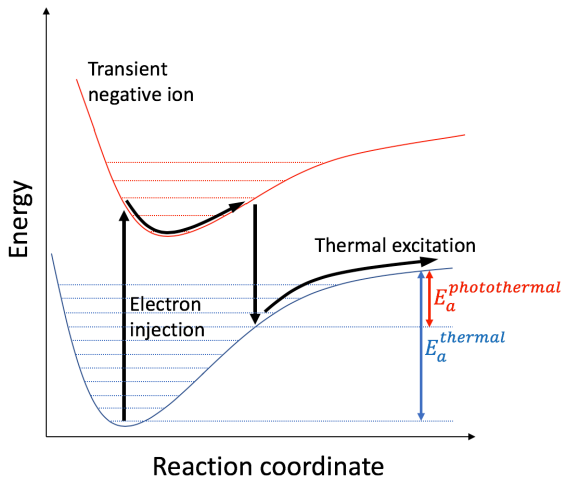

Fig. 3 Schematic of the photothermal process via a transient negative ion, which reduces the required thermal energy for the chemical reaction of the adsorbate

surface calculated with density functional theory (DFT) at the O_2 equilibrium geometry accurately matched the plasmon energy, supporting the notion that an electron is transferred from the metal to the adsorbate. The electron from the metal occupies the empty $2\pi^*$-antibonding orbital in this case. Kinetic isotope studies using labelled oxygen showed that the kinetic isotope effect (KIE), the ratio of reaction rates for $^{16}O_2$ and $^{18}O_2$, was higher for the photoinduced process than for the thermal (light off) process, which confirms that the O_2 dissociation step is the RDS. Figure 3 shows how both plasmons and the thermal bath may contribute to the dissociation reaction of O_2. With an electron injected to a neutral oxygen molecule, O_2^- is formed at a non-equilibrium geometry, with an excited vibrational level. Therefore, the anion undergoes vibrational motion before being relaxed to the neutral state, and the geometry is off-equilibrium after the molecule ejects an electron. This process of gain and then loss of an electron deposits energy in the O–O vibrational mode, which reduces the thermal energy required to cause dissociation. This means the temperature of the photocatalysis process for a comparable reaction rate is lower than the thermal process. The KIE also supports this mechanism; because the vibrational frequency of $^{16}O_2^-$ is higher than $^{18}O_2^-$ due to the mass difference, the nuclear displacement of $^{16}O_2^-$ is larger than $^{18}O_2^-$ before losing an electron relaxing to the neutral state. This leaves $^{16}O_2$ in a higher vibrational level, leading to a higher dissociation rate, which is consistent with the experimental result.

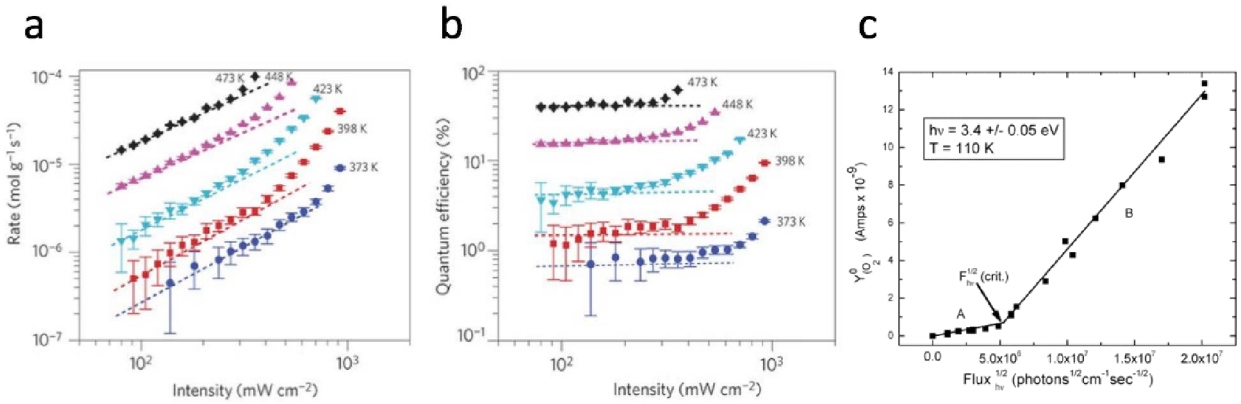

Fig. 4 (**a**) The rate of ethylene oxide formation (in log scale) on Ag nanocubes supported by α-Al_2O_3 as a function of the intensity of the incident light (in log scale) for various temperatures. (**b**) Calculated quantum efficiency from the same experiment. (**c**) The rate of O_2 desorption from TiO_2(110) as a function of the square root of the incident light flux. Reprinted from: **a**,**b,** [38] © 2012 Nature Publishing Group; **c**, [39] © 2005 American Chemical Society

Plasmonic photocatalysis has many useful features compared to conventional semiconductor photocatalysis. Importantly, there is a much lower activation energy when the adsorbates are on metal particles than on semiconductors, leaving only little energy that has to be overcome for chemical transformations to occur.[13] The other factor is dependence of the catalytic activity on the incident light intensity. In Fig. 4a and 4b, the reaction rate and calculated quantum efficiency of t he ethylene oxide formation reaction catalyzed by 75-nm edge Ag nanocubes supported on α-Al_2O_3 particles are plotted against incident light intensity for different temperatures. There is a linear (at moderate intensity) to supralinear (at high intensity) dependence of the reaction rate on the incident light intensity, and this means the quantum efficiency increases as a function of the light intensity, which is attributed to the possibility of multi-photon excitation of the adsorbate. In contrast, semiconductor catalysis exhibits a sub-unity order dependence on the incident light intensity (However, plasmon-assisted semiconductor photocatalysis shows a linear dependence of reaction rate on incident light flux. See below). It has been shown experimentally that O_2

desorption reaction from a TiO_2 surface has a ½-order dependence above a critical light intensity (Fig. 4c). Theory work indicates that this is because charge carriers generated in the bulk predominantly relax through charge recombination.[39, 40] The half-order dependence is the result of the second-order kinetics in charge carrier concentration in the bulk semiconductor, while the rate scales linearly in charge carrier concentration on the surface.[41] It was also observed that in an aqueous suspension of TiO_2, oxidation of formate follows a 0.61-order dependence.[42] The seemingly random number of 0.61 is probably influenced by multi-hole transfer to the reactant and multiple elementary steps in the overall reaction kinetics.

Although it is primarily the plasmonic response of the metal NP that greatly increases the reaction rate in photothermal catalysis, the role of the thermal bath must be carefully considered in the overall reaction.[44] As seen in Fig. 5, in plasmonic photocatalysis reactions, the reaction rate monotonically increases with temperature, while most semiconductors exhibit the opposite trend after some critical point, due to the faster multiphonon nonradiative charge carrier recombination at higher temperature (characterized by the Debye temperature). The faster reaction rate at higher temperature in plasmonic photocatalyzed reactions may be attributed to a number of factors. First, the

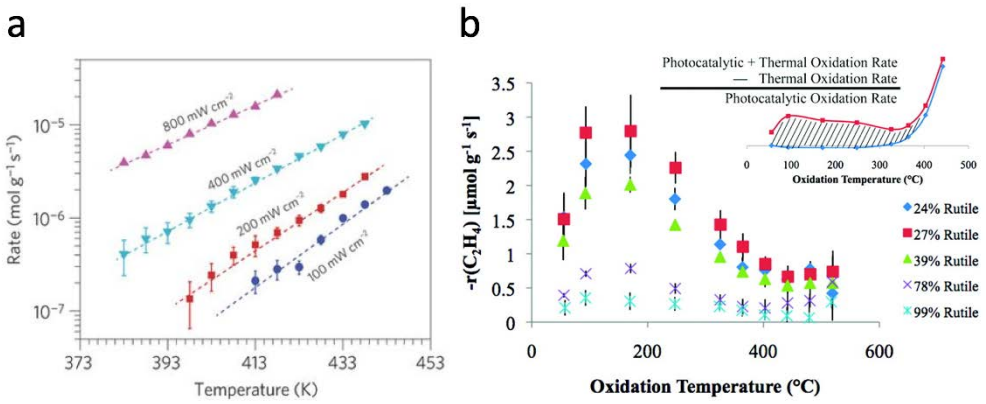

Fig. 5 (**a**) Rate of ethylene oxidation reaction (in log scale) on Ag nanocubes supported by α-Al_2O_3 as a function of operating temperature for various incident light intensities. (**b**) Rate of the same reaction on five different forms of TiO_2 as a function of operating temperature. Photocatalytic rate was calculated by subtracting the thermal oxidation rate (without light) from the total oxidation rate (with light). Reprinted from: **a**, [38] © 2012 Nature Publishing Group; **b**, [43] © 2011 American Chemical Society

thermal bath directly contributes to the energy gaining process through gain and loss of an electron (see above), since the electron transfer rate from the metal particle to the adsorbate is higher for adsorbates that are more vibrationally excited.[45] Second, with the plasmonic contribution to the dissociation step, the thermal energy required for the subsequent elementary steps may be greater than the dissociation step, enabling one of these steps to control the overall reaction rate. In this case, the increased charge recombination rate due to the higher temperature becomes less relevant to the overall reaction rate. Third, removal of the product may exclusively depend on vibrational energy from the thermal bath. Because catalysis may be the most efficient at plasmonic hot spots, removal of the end-product is essential before introduction and catalysis of a new reactant molecule. Fourth, phonon transfer from the thermal bath leads to a Boltzmann distribution of vibrational states, which gives a range of vertical energy difference between the neutral and the excited state. This may better utilize the finite bandwidth of the light source.

When the plasmons decay, hot holes as well as hot electrons are generated and can be used for chemical reactions. For example, citrate molecules attached to Au NPs on an indium tin oxide (ITO) substrate[46] and Ag NPs on a various substrates[47] undergo oxidation reactions (photo-Kolbe reaction) when weakly irradiated.

Another type of plasmon driven photochemical reaction is the photocatalyzed size growth of plasmonic particles. Photoinduced conversion of Ag nanospheres to nanoprisms was reported in 2001.[48] In addition, when the nanospheres are irradiated with light whose wavelength matches the dipole resonance wavelength of the prisms, a bimodal distribution of nanoprism sizes was obtained, suggesting that the plasmon drives fusion of the prisms. In a subsequent work, a

unimodal fabrication was done by using two wavelengths simultaneously, one at the dipole and the other at the quadrupole resonance wavelength.[49] This implies that prism fusion can be inhibited when quadrupole modes are excited. In another work, photoreduction of aqueous Ag ions on an immobilized array of Au NPs was reported.[50] Here it was found that the thickness of the deposited Ag layer was larger in the peripheral region, where the laser beam was not irradiated. This was explained as hot electrons conducting along the Ag pathways generated as a result of the deposition.

Lastly, some points that merit further study are noted. First of all, whether plasmons decay before charge transfer occurs is not clear. Figure 6 describes two possible mechanisms of electron transfer from the plasmonic metal to the ligand molecule. One is that plasmons generated in the Au NP decay to give hot electrons and holes which form a Boltzmann distribution, then hot electrons of high enough energy comparable to the unoccupied orbital energy level of the adsorbate molecule are transferred generating transient anions, leading to further reactions (Fig. 6a). On the other hand, it is possible that plasmons directly interact with the adsorbate and resonant transfer occurs (Fig. 6b). Also, reaction pathways that

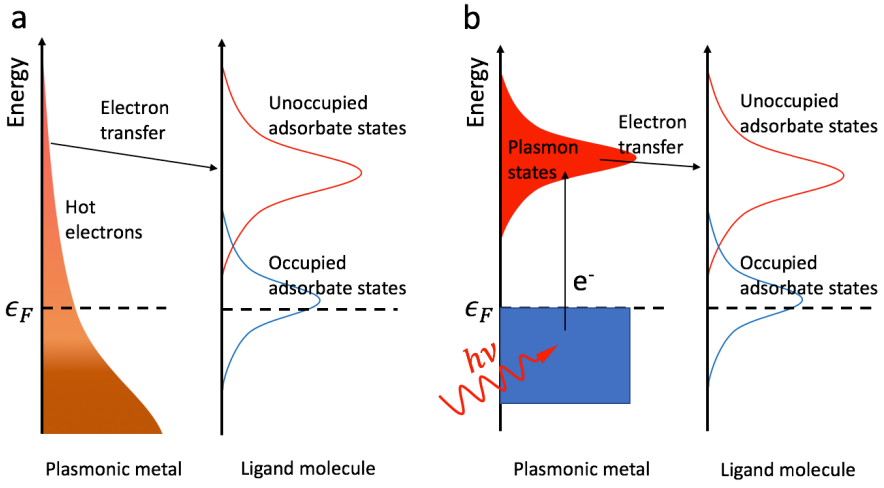

Fig. 6 Proposed electron transfer mechanism via (**a**) hot electron generation (**b**) direct interaction between plasmons and unoccupied states of the ligand. The horizontal dashed line designates the Fermi level (ϵ_F). Adapted from: **a**, [36] © 2013 American Chemical Society; **b**, [13] © 2011 Nature Publishing Group

result from the transient anion species after electron transfer are often unknown. For example, in the H_2 dissociation photocatalysis near a Au NP, H_2^- may dissociate and then eject an electron; otherwise, it may relax to the neutral state and then dissociate. Studies to uncover these mechanistic details are important to further understand plasmonic photocatalysis, and will need time-resolved spectroscopy and/or computational reaction dynamics studies.

5.2.2 Photocatalysis by Composite Metal–Semiconductor Structures

High-efficiency water splitting catalysis is economically and environmentally important since it can reduce reliance on fossil fuels. Although photoactivity of TiO_2 such as its ability to photo-bleach dyes and to oxidize organic solvents under UV irradiation has been reported in the scientific community since the early 20th century, it has been the object of extensive studies only since 1970s when it was reported[52] in 1972 (originally in 1969 in Japanese[53]) that water photolysis under sunlight is possible using an n-type TiO_2 electrode connected to a Pt counter-electrode through an external circuit.[54] Since then, many metal oxide, (oxy)sulfide, and (oxy)nitride photocatalysts for water splitting have been reported. A thorough review was published that overviews the materials and the system setups for these photocatalysts.[55]

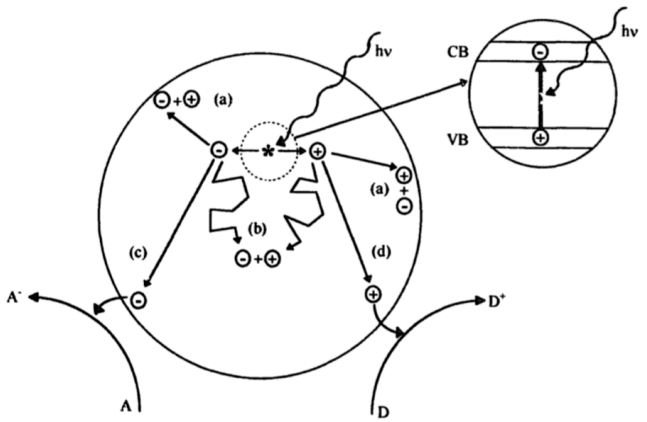

Fig. 7 Semiconductor photocatalysis scheme. With an incident photon ($h\nu$) impinging on the semiconductor, electrons are excited from the valence band (VB) to the conduction band (CB), generating hot electrons and holes. They can undergo charge recombination (a) near the surface of the semiconductor or (b) in the bulk, dissipating energy as heat. Electrons and holes that diffuse to the semiconductor/solvent interface can participate in (c) reduction and (d) oxidation reactions, respectively. A and D stand for the electron acceptor and donor, respectively. Reprinted from [51] © 1997 Elsevier

In semiconductor systems (Fig. 7), electron–hole pairs are generated when the light is absorbed in the semiconductor, and each charge carrier separates and diffuses to the catalytically active site at the interface of the semiconductor and solvent. Electrons and holes may recombine at trap sites caused by defects in the bulk or on the surface. In water splitting, the electrons and holes participate in the hydrogen evolution and the oxygen evolution half-reactions, respectively, which can be described at low pH in terms of the reactions

$$2H^+ + 2e^- \rightarrow H_2$$

$$H_2O + 2h^+ \rightarrow 2H^+ + \frac{1}{2}O_2.$$

While semiconductor photocatalysis is very appealing, it suffers from a number of factors for practical use. The band gap may be too large such that only a narrow region of the solar spectrum can be utilized; for example, TiO_2 has a 3.2 eV band gap, which means only UV light can generate electron–hole pairs in TiO_2. Also, the diffusion rate of the charge carriers is often not high enough that most charge carriers relax through charge recombination before reaching the reaction sites. Moreover, semiconductors may have poor catalytic activity, i.e., the activation energy may be too high at the semiconductor–solvent interface for the catalysis to be useful.

It has been demonstrated that these limitations can be partially lifted by using composite plasmonic metal–semiconductor systems and much higher reaction rates are achieved compared to their semiconductor-only counterpart.[56-71] The most important example of a plasmonic metal used with a semiconductor is as the sensitizer for visible light. For instance, García and coworkers tested various gold loading and calcination temperatures for Au/TiO_2 catalysts for water splitting and obtained a maximum quantum yield of 7.5% for H_2 and 5.0% for O_2 at a

visible wavelength (560 nm), while using a TiO_2 catalyst without plasmonic metal at the same wavelength resulted in quantum yields of less than 0.1%.[57] This is because the utilized wavelength is consistent with the dipole resonance frequency of Au NPs (spheres) but is too long compared to the band gap of TiO_2. It is important to harvest visible light in photocatalysis because while UV light constitutes less than 10% of the solar energy that reaches the surface of Earth, visible light accounts for around a half of the total energy. Moreover, a broad range of the solar spectrum can be utilized with plasmonic NPs since resonance frequencies of plasmonic NPs are tunable by changing shape, size, and dielectric environment. One can imagine using NPs having a range of size to maximize the utilized wavelength range.

Photocatalysis mechanism in the composite systems falls into one of two categories depending on the wavelength of the light source that when the photon energy is comparable to the band gap of the semiconductor charge carriers are generated directly in the semiconductor and the plasmonic metal merely serves as reaction sites and when plasmons in the metal can be excited plasmon-enhanced chemistry is relevant.[57] The two mechanisms can act together in one system, although one may be more dominant depending on the wavelength. In the processes that involve plasmons, the role of the metal around the semiconductor

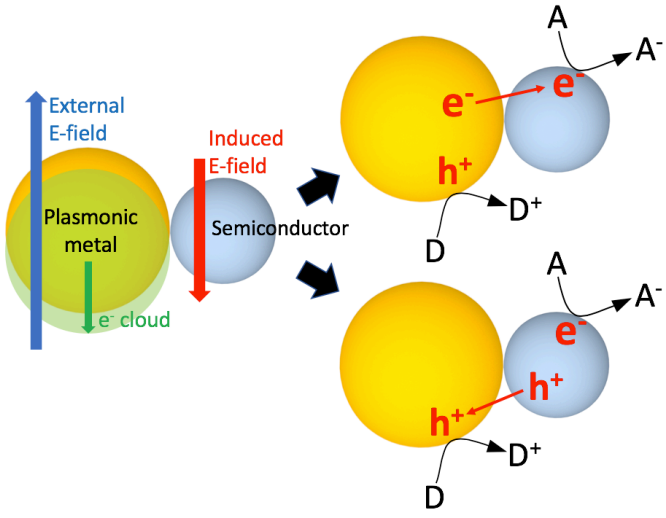

Fig. 8 Two possible mechanisms (charge injection and EM enhancement) of plasmon-mediated semiconductor photocatalysis. D and A stand for electron donor and acceptor, respectively.

is twofold: (1) It generates charge carriers which are transferred to the semiconductor (charge injection), and (2) it increases the charge separation rate inside the semiconductor near the surface by enhancing the electromagnetic field (EM enhancement). Figure 8 schematically describes these two mechanisms. In either case, the first step involves generation of plasmons within the plasmonic metal by the external EM field. Then, on one hand, the plasmons can decay to give electron–hole pairs in the plasmonic metal. On the other hand, the EM field inside the semiconductor amplified by the scattered field resulting from plasmon excitation can induce electron–hole pair generation near the surface of the semiconductor,[58, 59, 67, 71, 72] where the EM field intensity is high. While charge carriers generated in the bulk have to migrate to the surface to participate in chemical reactions and in the meantime are subject to charge recombination at defect sites, electrons and holes generated near the surface have a higher probability to survive until reaching the reaction sites. Charge carriers may transfer between the metal and semiconductor depending on their kinetic energy and on the relative energy levels of the valence/conduction bands of the two components.

Plasmon-assisted photocatalysis has been observed in systems where the semiconductor is separated from the plasmonic metal by a non-conductive spacer, preventing charge transfer between the two phases.[58, 59, 67, 71] Also, the source wavelength had to match the band gap of the semiconductor for the catalysis to occur. These observations support the EM mechanism. One prominent example by Awazu et al.[58] related to this mechanism is shown in Fig. 9 and 10. Here, Ag NPs coated with a SiO_2 shell were deposited on a TiO_2 film, and the entire structure was supported by a SiO_2 layer. The decomposition rate of methylene blue under near-UV light

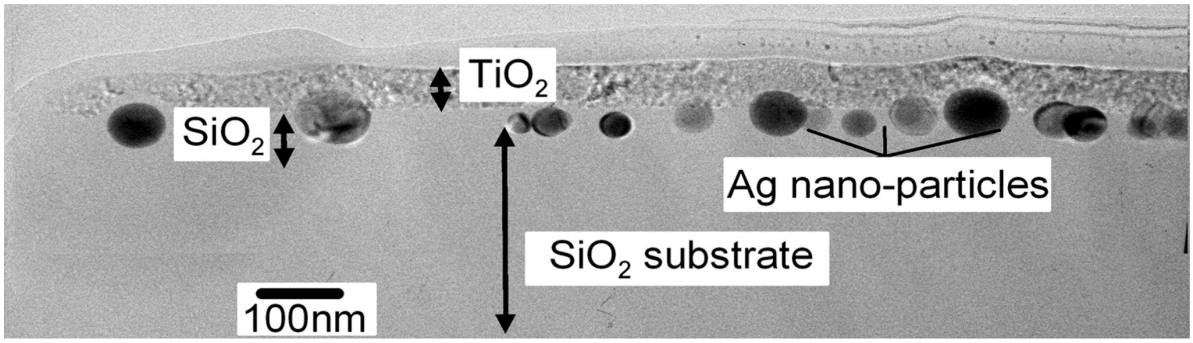

Fig. 9 Transmission electron microscopy (TEM) image of Ag/SiO_2 core–shell structures embedded in TiO2 film supported by SiO_2 substrate, which was used in photocatalytic decomposition of methylene blue. Reprinted from [58] © 2008 American Chemical Society

was shown to be faster in the presence of Ag NPs, supporting the field-enhancement mechanism by plasmon excitation.

5.3. Theoretical Studies of Plasmon-Enhanced Chemistry

Theory concerned with plasmon-enhanced chemistry has progressed in a number of directions,[3, 10, 16, 17, 25, 27, 73-79] as this is a field with many challenges and no single theory is going to solve all problems. Very recently, Zhang et al.[2] developed a nonadiabatic molecular dynamics approach based on time-dependent density functional theory (TDDFT) for the excited stated dynamics of a system consisting of a metal NP and a ligand molecule (taken to be H_2), and showed that this treatment correctly describes hot-electron transfer from the

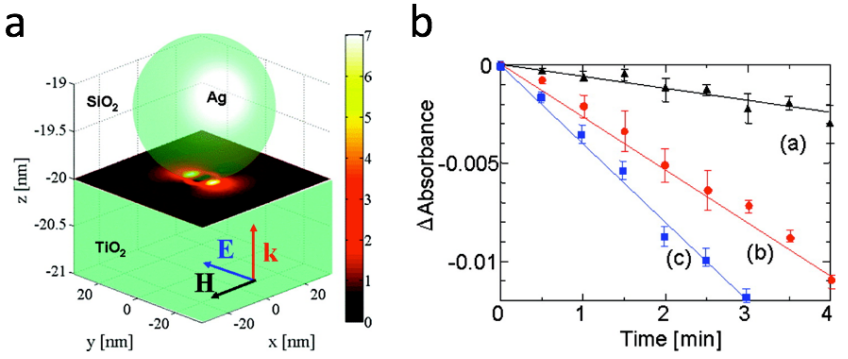

Fig. 10 (**a**) FDTD simulation result showing enhanced electric field amplitude at 400 nm shortly below the TiO_2–SiO_2 interface due to a 40-nm Ag nanosphere on the TiO_2 film. The Ag nanosphere is not drawn to scale. (**b**) Decomposition rate of methylene blue under near-UV irradiation monitored at the wavelength of 580 nm, on (a) a TiO_2 film on a SiO_2 substrate (b) a TiO_2 film on a Ag/SiO_2 core–shell structure with shell thickness of 20 nm on a SiO_2 substrate (c) a TiO_2 film on a Ag/SiO_2 core–shell structure with shell thickness of 5 nm on a SiO_2 substrate. Figures reprinted from [58] © 2008 American Chemical Society

metal particle to the ligand followed by dissociation of the ligand. This approach treats all the electrons in the system, and therefore both the plasmons and the dissociative molecular states with quantum mechanics (QM), and only nuclear motion is approximated with classical molecular dynamics. However, current computational power limits the size of the system to a few hundred atoms, which means the particles are at most only a few nm in size. This is far smaller than the experiments, and thus the plasmons can be blue-shifted from the actually utilized plasmonic wavelength. Also, to reduce the overall timescale for the calculations, it was necessary to use high light intensities in these calculations and a jellium approximation for the metal electrons.

The alternative approach to using QM to describe metal particle optical excitation is to use classical electrodynamics (ED), namely Maxwell's equations. This has the advantage of being applicable to the large metal NPs that are used in most experiments. The review by Zhao et al.[80] gives an overview of analytical and numerical methods that are commonly used, including Mie theory, the quasistatic model for spheres and spheroids, the discrete dipole approximation (DDA), the finite-difference time-domain (FDTD) method, and the finite element method (FEM). However, these methods do not consider electron transfer between the metal particles and the ligand molecules, leading to omission of plasmonic photocatalysis as well as changes in the electronic structure of the ligand due to the presence of the metal NPs. This latter effect leads to the chemical mechanism (CM) in SERS and is likely also involved in plasmon enhanced chemical reactions.

In-between the quantum mechanical and the classical electrodynamic limit is the QM/ED hybrid theories. In one version, one can calculate the electromagnetic (EM) response of the plasmonic particle and then apply the resulting field as driving a QM calculation for the ligand molecule. For example, FDTD method and RT(real-time)-TDDFT have been combined to calculate molecular optical properties of the absorption spectrum and the Raman spectrum in the time domain.[81] Also, frequency-domain linear response TDDFT has been used with the electric field computed from FDTD method as the perturbation to determine an enhanced effective polarizability, which was used in calculating the Raman spectra of pyridine and rhodamine-6G.[82] The shortcoming of these methods is that they omit the CM. One way to consider the CM is to explicitly include the metal cluster in the QM calculation. For instance, a QM calculation was done in a molecule–truncated Ag cluster system using the EM field obtained from Mie theory to obtain SERS and SEHRS spectra.[83] Here, it was shown that the CM is essential to correctly simulate SERS and SEHRS and that the frequency-dependence of the SERS/SEHRS spectrum of the gas-phase ligand molecule may be included for more accurate spectra.

There is also a coarse-grained EM model where the atoms or groups of atoms in the metal particle are parameterized as having induced dipoles and charges, with effective polarizabilities and hardness parameters that are fit using an iterative procedure where one matches the interaction between the ligand molecule and the metal particle.[84, 85] The external field is then considered as a perturbation in the linear-response TDDFT calculation. This model is useful for understanding spectroscopic properties such as SERS, but like standard ED, it does not describe the production of hot electrons.

5.4 Plasmon-Coupled Resonance Energy Transfer: Experiments

As mentioned in the introduction, PC-RET is an important process that often occurs in the same systems as plasmonic photocatalysis but can also be distinct. In this process, excitation is transferred from one molecule to another in the presence of a plasmonic NP, such that plasmon excitation serves as an important transport mechanism. Recent experiments[86-93] and theory[94-98] have provided important insights into this process, and in this Section of the Chapter we first review the recent literature and then provide a detailed discussion of the underlying theory.

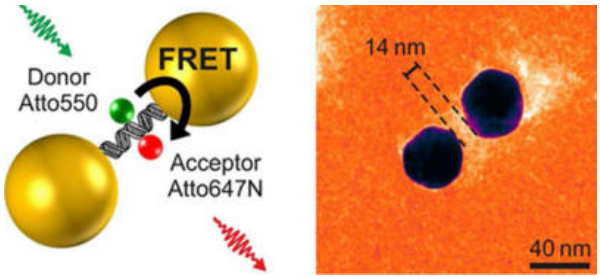

Fig. 11 Single donor–acceptor pair in a DNA-linked plasmonic dimer nanoantenna. Reprinted from [86] © 2016 American Chemical Society

Wenger and coworkers[86-88] have examined D–A transfer between dyes attached to DNA in the presence of Au nanostructures that influence both fluorescence and energy transfer. In one structure (Fig. 11), the DNA linked two Au nanospheres that are 40 or 60 nm in diameter with a 14 nm gap, the D–A distance being 4 nm. In another study,[87] the DNA was randomly located in 160-380 nm nanoholes in a Au film that was 150 nm thick. The structure in the first study was better defined, but the D–A distance was not varied, while in the second, the D–A distances were varied between 2.4 and 13.6 nm, and significant deviations from the quasistatic R^{-6} distance dependence were found. By varying nanosphere diameter or hole size and also performing fluorescence and RET studies in solution, it was possible to determine the plasmon enhancement effect on both donor and acceptor emission, and on PC-RET. In the first study the

RET rate was found to increase by a factor of 5 with Au particles present, but it was also found that donor emission was enhanced by more than this, indicating weak transfer efficiency. In the second study, the RET rate was found to increase by a factor of 6 for the case of 13.6 nm separation and 160 nm holes compared to the same separation and no hole, thereby demonstrating the importance of the plasmon enhanced local density of states on RET.

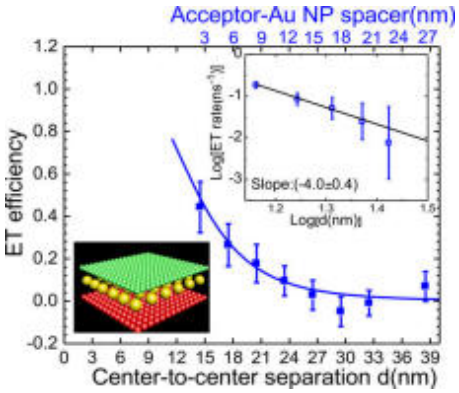

Fig. 12 Schematic of trilayer involving donor(green), Au NP (yellow), acceptor (red). Data shows energy transfer efficiency as function of D–A separation, including log plot. Reprinted from [89] © 2014 American Chemical Society

Another relevant class of experiments related to PC-RET has been presented by Bradley and coworkers.[89] Figure 12 shows the basic structure, in which one has layers of donor and acceptor quantum dots (CdTe particles with diameters of 2.6 and 3.4nm, respectively) that are separated by a polyelectrolyte spacer from a layer of 5.0 nm Au NPs. D–A distances up to 38 nm were considered, with the Au NP layer resulting in significantly longer-range energy transfer (up to 30 nm compared to 9 nm without). The results were interpreted in terms of a theory that included the full electrodynamic response, using a generalized Mie approach for the spheres in the Au layer, but with the constraint that only a finite number of spheres could be included (and most of the modeling was done with just one sphere).

A related experimental study by the Bradley group was presented by Zhang et al.,[90] who studied RET involving CdTe quantum dots as donors and a sheet of Au NPs as acceptors, separated by a layer of polyelectrolyte of controllable thickness up to 21 nm. In this case the Au

NPs act as absorbers with a characteristic absorption spectrum that is dictated by plasmon excitation. Also, by changing the size of the CdTe particles it was possible to tune the spectrum of CdTe compared to the plasmon and therefore to control the spectral overlap function. The authors found that there was a better fit of their results to a dipole–sheet (continuous sheet) energy transfer model than to the usual Förster dipole–dipole model, with the largest deviations being associated with the largest D–A distances.

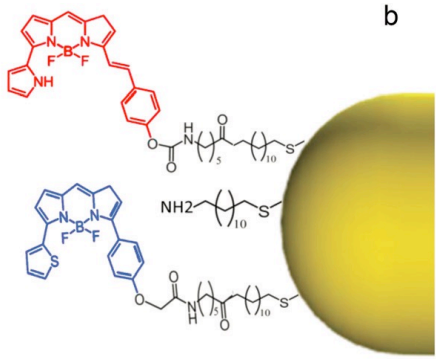

Fig. 13 Donor (blue)–acceptor (red) molecules that are tethered to a Au nanorod. Reprinted from [99] © 2017 Royal Society of Chemistry

Another type of PC-RET experiment was recently reported by Bujak et al.[91] Here, the donor and acceptor molecules were chemically tethered to the end of a Au nanorod (Fig. 13), and D–A energy transfer was observed for individual nanorods near 615 nm as a function of the direction of the light polarization relative to the rod axis direction. The D–A separation distance was not controlled, however emission by the acceptor was found to be higher (estimated to be a factor of 65) for parallel polarization, which could excite the longitudinal rod plasmon. Fluorescence from both donor and acceptor was observed for polarizations parallel and perpendicular to the rod axis, and also for D–A pairs adsorbed on nonplasmonic particles. It was found that only for the rod did the ratio of D and A fluorescence vary with polarization, which is a signature of PC-RET. The results were interpreted using a PC-RET approach from Pustovit[100], which is a version of the theory described in the next section but restricted to spherical particles and the quasistatic limit. The D–A separation was empirically adjusted to fit the data, which was found to be 16 nm.

5.5 Theoretical Studies of Plasmon-Coupled Resonance Energy Transfer

Some of the theoretical work on PC-RET was mentioned in the review above, especially as applies to specific Au nanostructures such as spheres or flat films. In this section we describe a general approach to the description of D–A energy transfer in the presence of a plasmonic nanostructure (or more generally an arbitrary inhomogeneous and dispersive dielectric structure), as has been recently developed by Schatz and coworkers.[94, 96, 97] Since this theory is relatively new, and further generalizations are still desired, this Section will provide a comprehensive examination of the underlying description of this phenomenon. In Section 5.5.1, general expressions for RET rate in an arbitrary dielectric environment based on the use of Green's functions are derived within classical and quantum mechanical pictures. In Section 5.5.2, key characteristics of PC-RET that are revealed by this formulation are reviewed. Note that all equations below are in SI units.

5.5.1 Rate Expressions for Electric Dipole–Electric Dipole Resonance Energy Transfer

The rate expression for RET in an arbitrary dielectric environment based on classical electrodynamics (CED) is [110]

$$\frac{\gamma_{D\to A}^{CED}}{\gamma_0} = 18\pi \int_0^\infty d\omega \left|\boldsymbol{n}_A^\dagger \overleftrightarrow{G}(\boldsymbol{r}_A, \boldsymbol{r}_D; \omega)\, \boldsymbol{n}_D\right|^2 \sigma_A(\omega)\, I_D(\omega), \quad (1)$$

where $\gamma_0 = \frac{\omega_0^2 |\boldsymbol{p}_D|^2}{3\pi\epsilon_0 \hbar c^3}$ is the donor decay rate in free space without the acceptor, ω_0 is the electronic transition frequency, $\sigma_A(\omega)$ is the absorption cross-section of the acceptor, $I_D(\omega)$ is the area-normalized emission spectrum of the donor, $\boldsymbol{n}_{D(A)} = \frac{\boldsymbol{p}_{D(A)}}{|\boldsymbol{p}_{D(A)}|}$ is the unit vector in the direction of

the donor (acceptor) dipole moment, and $\boldsymbol{r}_{D(A)}$ is the position of the donor (acceptor) dipole. The dagger symbol means the conjugate transpose. The dyadic Green's function $\overleftrightarrow{G}$ is defined as the solution of

$$\nabla \times \nabla \times \overleftrightarrow{G}(\boldsymbol{r}, \boldsymbol{r}'; \omega) - k_0^2 \epsilon(\boldsymbol{r}, \omega) \overleftrightarrow{G}(\boldsymbol{r}, \boldsymbol{r}'; \omega) = \overleftrightarrow{I}\, \delta(\boldsymbol{r} - \boldsymbol{r}'), \quad (2)$$

where $k_0 = \frac{\omega}{c}$, $\epsilon(\boldsymbol{r}, \omega)$ is the relative permittivity in the frequency domain, I is the unit dyad, and δ is the Dirac delta function. Analytical or numerical computation of $\overleftrightarrow{G}$ may be complicated, but this can be circumvented by using the relation $\boldsymbol{E}_D(\boldsymbol{r}, \omega) = \int_V \overleftrightarrow{G}(\boldsymbol{r}, \boldsymbol{r}'; \omega)\, i\omega\mu_0 \boldsymbol{j}_s(\boldsymbol{r}') d\boldsymbol{r}'$, where $\boldsymbol{j}_s$ is the electric current of the source and μ_0 is the vacuum permeability. This arises from

$$\nabla \times \nabla \times \boldsymbol{E}_D(\boldsymbol{r}, \omega) - k_0^2 \epsilon(\boldsymbol{r}, \omega) \boldsymbol{E}_D(\boldsymbol{r}, \omega) = i\omega\mu_0 \boldsymbol{j}_s(\boldsymbol{r}), \quad (3)$$

which is a direct consequence of Maxwell's equations. Here, $\boldsymbol{E}_D$ is the sum of the direct electric field from the source and the response electric field of the environment. Note that the relative permeability is assumed as 1 in all space in Eq. (2) and (3). For a dipole source, $\boldsymbol{j}_s(\boldsymbol{r}) = -i\omega \boldsymbol{p}_D \delta(\boldsymbol{r} - \boldsymbol{r}_D)$, so $\boldsymbol{E}_D = \omega^2 \mu_0 \overleftrightarrow{G}(\boldsymbol{r}, \boldsymbol{r}_d; \omega)\, \boldsymbol{p}_D$. Using this, the RET rate expression becomes

$$\frac{\gamma_{D\to A}^{CED}}{\gamma_0}(\omega) = \frac{18\pi}{\mu_0^2} \int_0^\infty d\omega \frac{1}{\omega^4} \frac{\left|\boldsymbol{n}_A^\dagger \boldsymbol{E}_D(\boldsymbol{r}_A, \omega)\right|^2}{|\boldsymbol{p}_D|^2} \sigma_A(\omega)\, I_D(\omega). \quad (4)$$

$\boldsymbol{E}_D$ is a much easier quantity to calculate numerically and analytically than $\overleftrightarrow{G}$. In the special case of a homogenous environment with the relative permittivity $\epsilon_b(\omega)$ and where the D–A distance is small compared to the wavelength, the rate expression reduces to $\frac{\gamma_{D\to A}}{\gamma_0} = \frac{9c^4\kappa^2}{8\pi R^6} \int_0^\infty d\omega \frac{f_D(\omega)\sigma_A(\omega)}{\omega^4 \epsilon_b(\omega)^2}$, where $\kappa^2 = \left|\boldsymbol{n}_A^\dagger \boldsymbol{n}_D - 3\left(\boldsymbol{n}_A^\dagger \boldsymbol{n}_R\right)\left(\boldsymbol{n}_R^\dagger \boldsymbol{n}_A\right)\right|^2$ and $\boldsymbol{n}_R$ is the unit vector in the direction of $\boldsymbol{R} = \boldsymbol{r}_A - \boldsymbol{r}_D$. In many applications, orientation averaging of the donor and the

acceptor is done for real dipole moments, reflecting the random orientations of molecules, which gives $\kappa^2 = \frac{2}{3}$.

A derivation with quantum electrodynamics (QED) in the weak interaction limit and under the Born–Oppenheimer approximation results in essentially the same expression as CED. Using Fermi's golden rule, the RET rate as derived by Dung et al.[111] can be expressed as

$$\frac{\gamma_{D\to A}^{QED}}{W_D^r} = 18\pi \int_0^\infty d\omega \left|\boldsymbol{n}_A^\dagger \overleftrightarrow{G}(\boldsymbol{r}_A, \boldsymbol{r}_D; \omega)\, \boldsymbol{n}_D\right|^2 \sigma_A(\omega)\, I_D(\omega) \quad (5)$$

or

$$\frac{\gamma_{D\to A}^{QED}}{W_D^r}(\omega) = \frac{18\pi}{\mu_0^2} \int_0^\infty d\omega \frac{1}{\omega^4} \frac{\left|\boldsymbol{n}_A^\dagger \boldsymbol{E}_D(\boldsymbol{r}_A, \omega)\right|^2}{|\boldsymbol{p}_D|^2} \sigma_A(\omega)\, I_D(\omega), \quad (6)$$

where the absorption cross-section and the normalized emission spectrum expressions are [112, 113]

$$\sigma_A(\omega) = \frac{\pi\omega}{3\hbar\epsilon_0 \alpha_A c} \sum_{a,a^*} P_a\, |\boldsymbol{p}_A|^2 |\langle \chi_{a^*} \mid \chi_a \rangle|^2 \delta(\omega - \omega_{aa^*}) \quad (7)$$

$$I_D(\omega) = \frac{\alpha_D \omega^3}{3\pi\hbar\epsilon_0 c^3 W_D^r} \sum_{d,d^*} P_{d^*}\, |\boldsymbol{p}_D|^2 |\langle \chi_d \mid \chi_{d^*} \rangle|^2 \delta(\omega - \omega_{dd^*}), \quad (8)$$

where W_D^r is the total emission rate of the donor in a homogeneous medium without the acceptor,

$$W_D^r = \int d\omega \frac{\alpha_D \omega^3}{3\pi\hbar\epsilon_0 c^3} \sum_{d,d^*} P_{d^*}\, |\boldsymbol{p}_D|^2 |\langle \chi_d \mid \chi_{d^*} \rangle|^2 \delta(\omega - \omega_{dd^*}), \quad (9)$$

$d(a)$ and $d^*(a^*)$ are respectively the vibronic states in the electronic ground state and the excited state of the donor (acceptor), P_i $(i = d^*, a)$ is the probability of the given vibrational state being occupied, χ_i $(i = d, d^*, a, a^*)$ is the nuclear wavefunction, and ω_{dd^*} and ω_{aa^*} are the transition

frequencies. α_A and α_D arethe real-valued refractive indices which account for the effect of the solvent on the averaged fields (which satisfies $\alpha_A \approx \alpha_D$ for the same type of solvent.[94]) In a homogenous environment, the RET rate can also be derived within the second-order perturbation theory approximation by considering intermediate states in which a photon emitted by the donor is confined in free space.[104, 114]

It is also possible to bypass the direct calculation of the dyadic Green's function by using a scalar Green's function in the quasistatic limit. A scalar Green's function $g(\boldsymbol{r}, \boldsymbol{r}'; \omega)$ is set to satisfy

$$-\nabla \cdot \epsilon(\boldsymbol{r}, \omega) \nabla g(\boldsymbol{r}, \boldsymbol{r}'; \omega) = \delta(\boldsymbol{r} - \boldsymbol{r}'), \quad (10)$$

which is an analogue of the Poisson's equation in electrostatics. Then the electric field can be derived as (See Appendix A for derivation.)

$$\boldsymbol{E}_D(\boldsymbol{r}, \omega) = -\frac{1}{\epsilon_0} \boldsymbol{p}_D \cdot \left(\nabla_{\boldsymbol{r}} \nabla_{\boldsymbol{r}'} g(\boldsymbol{r}, \boldsymbol{r}'; \omega) \right)_{\boldsymbol{r}' = \boldsymbol{r}_D}. \quad (11)$$

The PC-RET rate can be obtained by plugging this equation into Eq. (4) or (6). The advantage of this expression is that Eq. (10) is more easily solved than the dyadic Green's function counterpart Eq. (2) so that physical insights can be gained. Specific examples of the scalar Green's function for spherical particles are derived in Appendix B along with expressions for the dipole polarizability α^p and quadrupole polarizability α^Q of a sphere that is polarized by a dipole source,

$$\alpha^p = \epsilon_b \frac{\epsilon_m/\epsilon_b - 1}{\epsilon_m/\epsilon_b + 2} a^3 \quad (12)$$

$$\alpha^Q = \epsilon_b \frac{\epsilon_m/\epsilon_b - 1}{\epsilon_m/\epsilon_b + \frac{3}{2}} a^5, \quad (13)$$

where a is radius of the sphere and ϵ_m and ϵ_b are relative permittivity of the sphere and the background medium, respectively. These are of the same form as when the source is a plane wave.[1, 110, 115]

5.5.2. Analysis of Plasmon-Coupled Resonance Energy Transfer

Eqs. (4) and (6) opens up a way to obtain PC-RET rates by calculating the electric field generated by the source dipole, which can be easily done for any dielectric environment using analytical methods such as Mie theory (for spheres) or numerical methods such as the FDTD method, FEM, and boundary element method (BEM). In these formulas, the coupling factor (CF) between the donor and the acceptor dipole, defined as $\frac{\left|\boldsymbol{n}_A^{\dagger}\,\boldsymbol{E}_D(\boldsymbol{r}_A,\omega)\right|^2}{|\boldsymbol{p}_D|^2}$, reflects the response field of the environment, and thus is more general than the R^{-6} factor associated with Förster resonance energy transfer theory[116]. Thus in PC-RET, the energy transfer rate is determined by the spectral overlap of three factors (termed the 'generalized spectral overlap'): the donor emission, the

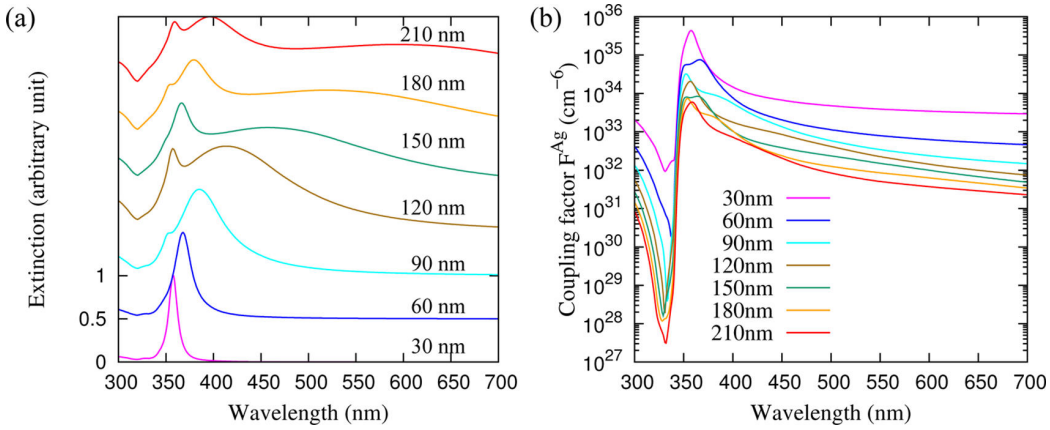

Fig. 14 (**a**) Normalized extinction spectra of spherical Ag nanoparticles with various sizes. (**b**) CF spectra of PC-RET in the presence of Ag nanospheres with various sizes, where the D–A pair is located diametrically, pointing radially, and separated from the metal surface by 10 nm. Reprinted from [97] © 2018 American Chemical Society

acceptor absorption, and the CF. Interestingly, because the CF is a complex function of system geometry, depending on positions and orientations of the donor and acceptor and on the particle shape and size, the CF spectrum may be fundamentally different in its frequency dependence from the extinction spectrum of the involved plasmonic metal nanostructure.[94] For example, for large spherical plasmonic nanoparticles, the dipole plasmon mode that often dominates in the extinction spectrum may appear only weakly in the CF spectrum, especially when the D–A pair are diametrically located around the sphere. This is illustrated for Ag spheres in Fig. 14 [97] where we see that in contrast to the extinction spectrum (Fig. 14a), the CF (Fig. 14b) is dominated by plasmon modes near 350 nm, with only weak dependence on sphere size. (See also Appendix C). Another important feature of PC-RET is that energy transfer may be slow when there is destructive interference between the direct field (i.e., that emitted by the donor) and the response field of the environment (i.e., of the nearby nanoparticle) because both fields add coherently, and may interfere, when they reach the acceptor dipole.[97] This may result in suppression of RET by the plasmonic metal.

5.6. Conclusion

In this chapter, plasmon-coupled photocatalysis and PC-RET were reviewed from both experimental and theoretical perspectives. As both areas are evolving fast, it is expected that in the years to come new types of photocatalysis reactions and promising applications benefiting from the PC-RET theory will emerge (For example, the PC-RET theory can be used to design exciton transport in metal–organic frameworks (MOFs)[117], solar cells[118-120], molecular imaging[121], molecular sensing[122, 123], and plasmonic nanowaveguides[124, 125].) However, it should be noted that many plasmon-coupled processes that compete with each other can be

present in one system,[86, 92, 93], which must be carefully considered when making predictions or giving an analysis of device performance.

Appendix A. Derivation of Quasistatic Expression of Electric Field from an Electric Dipole

To extract the electric field from the scalar Green's function, first, the electric potential $\Phi_{\mathrm{D}}(\boldsymbol{r})$ is obtained by integrating a product of the Green's function and the source term, which is the charge density, i.e,

$$\Phi_{\mathrm{D}}(\boldsymbol{r},\omega) = \int_{all\ space} d\boldsymbol{r}'\, g(\boldsymbol{r},\boldsymbol{r}';\omega)\frac{\rho_s(\boldsymbol{r}',\omega)}{\epsilon_0}. \quad \text{(A1)}$$

Using the source charge of the source dipole $\rho_s = -\boldsymbol{p}_D \cdot \nabla_{\boldsymbol{r}'}\delta(\boldsymbol{r}' - \boldsymbol{r}_D)$,

$$\Phi_{\mathrm{D}}(\boldsymbol{r},\omega) = \frac{1}{\epsilon_0}\int_{all\ space} d\boldsymbol{r}'\, g(\boldsymbol{r},\boldsymbol{r}';\omega)\big(-\boldsymbol{p}_D \cdot \nabla_{\boldsymbol{r}'}\delta(\boldsymbol{r}' - \boldsymbol{r}_D)\big)$$

$$= -\frac{1}{\epsilon_0}\boldsymbol{p}_D \cdot \int_V d\boldsymbol{r}' g(\boldsymbol{r},\boldsymbol{r}';\omega)\nabla_{\boldsymbol{r}'}\delta(\boldsymbol{r}' - \boldsymbol{r}_D), \quad \text{(A2)}$$

where V is a spatial region that the source dipole is located. For example, for a system of a source dipole outside of a NP, V is the outside region of the NP. With integration by parts, this transforms to

$$\Phi(\boldsymbol{r},\omega) = -\frac{1}{\epsilon_0}\boldsymbol{p}_d \cdot \Big(\int_S dS(-\hat{n})g(\boldsymbol{r},\boldsymbol{r}';\omega)\delta(\boldsymbol{r}' - \boldsymbol{r}_D) - \int_V d\boldsymbol{r}'\big(\nabla_{\boldsymbol{r}'}g(\boldsymbol{r},\boldsymbol{r}';\omega)\big)\delta(\boldsymbol{r}' - \boldsymbol{r}_D)\Big), \quad \text{(A3)}$$

where S is the surface between V and the rest of space and $\hat{n}$ is a unit vector normal to S, pointing to V. The first integral is zero because within S, $\boldsymbol{r}' \neq \boldsymbol{r}_D$. Evaluating the second integral results in

$$\Phi(\boldsymbol{r},\omega) = \frac{1}{\epsilon_0}\boldsymbol{p}_D \cdot \left(\nabla_{\boldsymbol{r}'} g(\boldsymbol{r},\boldsymbol{r}';\omega)\right)_{\boldsymbol{r}'=\boldsymbol{r}_D}. \quad \text{(A4)}$$

Applying $\boldsymbol{E}(\boldsymbol{r},\omega) = -\nabla_{\mathbf{r}}\Phi(\boldsymbol{r})$ leads to Eq. (11).

Appendix B. Dipole and Quadrupole Polarizability of a Sphere with a Dipole Source

For small enough particles or a source charge far from the NP, including plane wave, the scattered EM field can be approximated as that radiated from an induced electric dipole, perhaps with an induced quadrupole located at the center of the NP. A natural question is that whether the induced multipole moments can be calculated given the source charge. For a sphere, these quantities are reflected in the dipole polarizability α^p and the quadrupole polarizability α^Q defined as

$$\boldsymbol{p}_{ind} = 4\pi\epsilon_0\alpha^p \boldsymbol{E}_{inc}(\boldsymbol{r}_0) \quad \text{(B1)}$$

$$\overleftrightarrow{Q}_{ind} = 4\pi\epsilon_0\alpha^Q \left(\frac{\nabla \boldsymbol{E}_{inc}(\boldsymbol{r}) + \mathbf{E}_{inc}\nabla(\boldsymbol{r})}{2}\right)_{\boldsymbol{r}=\boldsymbol{r}_0}, \quad \text{(B2)}$$

where $\boldsymbol{r}_0$ is the center of the sphere and $(\nabla \boldsymbol{E})_{\alpha\beta} \equiv \frac{\partial E_\beta}{\partial \alpha}$ and $(\boldsymbol{E}\nabla)_{\alpha\beta} \equiv \frac{\partial E_\alpha}{\partial \beta}$ where $\alpha, \beta = x, y, z$. As seen in Eq. (B1) and B2, the induced dipole is the product of the dipole polarizability and the electric field at the center of the sphere, and the induced quadrupole is obtained as the product of the quadrupole polarizability α^Q and the symmetric part of the gradient of the electric field at the

center of the sphere.[126] For a plane wave source, α^p and α^Q are relatively well known (See below). For an electric dipole source in vacuum, Kerker et al.[127] showed that the induced dipole is determined in a similar way to the plane wave source case using the far-zone scattered field. Here, we derive the dipole and quadrupole polarizability of a spherical particle for an electric dipole source using Eq. (11).

Solving Eq. (10) for a sphere with the source charge outside of the sphere (i.e. $r' > a$) gives different forms of solution for $r > a$ and $r < a$. The solution outside of the sphere ($r > a$) is relevant when the scattered field is of interest. The solution in this region is [128, 129]

$$g(\boldsymbol{r}, \boldsymbol{r}'; \omega) = g^{direct}(\boldsymbol{r}, \boldsymbol{r}') + g^{scat}(\boldsymbol{r}, \boldsymbol{r}'; \omega), \quad \text{(B3)}$$

where

$$g^{direct}(\boldsymbol{r}, \boldsymbol{r}') = \frac{1}{4\pi\epsilon_b|\boldsymbol{r}-\boldsymbol{r}'|} \quad \text{(B4)}$$

$$g^{scat}(\boldsymbol{r}, \boldsymbol{r}'; \omega) = -\sum_{l=1}^{\infty}\sum_{m=-l}^{l} \frac{1}{2l+1}\frac{1}{\epsilon_b}\frac{l(\epsilon_m/\epsilon_b-1)}{l(\epsilon_m/\epsilon_b+1)+1}\frac{a^{2l+1}}{r'^{l+1}r^{l+1}} Y_{lm}(\theta,\phi)Y_{lm}^*(\theta',\phi'). \quad \text{(B5)}$$

where r, θ, ϕ are respectively the radius, polar angle, and azimuthal angle in the spherical coordinate system with the origin located at the center of the sphere. g^{direct} corresponds to the potential directly from the point source $\delta(\boldsymbol{r} - \boldsymbol{r}')$ and g^{scat} to the response potential from the sphere. For convenience, each multipolar contribution to the scattering response term is defined as

$$g_{lm}^{scat}(\boldsymbol{r}, \boldsymbol{r}'; \omega) = -\frac{1}{2l+1}\frac{1}{\epsilon_b}\frac{l(\epsilon_m/\epsilon_b-1)}{l(\epsilon_m/\epsilon_b+1)+1}\frac{a^{2l+1}}{r'^{l+1}r^{l+1}} Y_{lm}(\theta,\phi)Y_{lm}^*(\theta',\phi') \quad \text{(B6)}$$

so that

$$g^{scat}(\boldsymbol{r}, \boldsymbol{r}'; \omega) = \sum_{lm} g_{lm}^{scat}(\boldsymbol{r}, \boldsymbol{r}'; \omega). \quad \text{(B7)}$$

For simplicity, we assume that the source dipole is pointing radially from the sphere on the z axis. In this case, the relevant terms in Eq. (B5) are those with $m = 0$ for all l, since $m \neq 0$ components have ϕ-dependence while the potential contribution from the sphere should be independent of ϕ.

α^p and α^Q are obtained by equating the scattered electric field from the induced multipoles Eq. (B1) and B2 to the quasistatic scattered field expression Eq. (11). Using the electric field expression from an electric dipole in the quasistatic limit [110]

$$\boldsymbol{E}(\boldsymbol{r}) = \frac{1}{4\pi\epsilon_0}\frac{1}{\epsilon_b r^3}(3\boldsymbol{n}(\boldsymbol{n}\cdot\boldsymbol{p}) - \boldsymbol{p}), \quad \text{(B8)}$$

where $\boldsymbol{p}$ is the dipole moment, $\boldsymbol{n} = \frac{\boldsymbol{r}}{|\boldsymbol{r}|}$ is the unit vector from the dipole to the point where the electric field is measured, $r = |\boldsymbol{r}|$, and ϵ_b is the relative permittivity of the background medium, it is easy to show that the incident electric field at the center of the sphere from the donor dipole is $\boldsymbol{E}^{inc}(\boldsymbol{r}_0) = \frac{1}{4\pi\epsilon_0}\frac{2p_D}{\epsilon_b r_D^3}\hat{z}$, and therefore the induced dipole moment is $\boldsymbol{p}^{ind} = \frac{2\alpha^p p_D}{\epsilon_b r_D^3}\hat{z}$. Plugging this in Eq. (B8) results in the scattered field from the induced dipole

$$\boldsymbol{E}_p^{ind}(\boldsymbol{r}) = \frac{1}{4\pi\epsilon_0}\frac{2\alpha^p p_D}{\epsilon_b^2 r_D^3 r^3}(\hat{r}\, 2cos\theta + \hat{\theta}\, sin\theta). \quad \text{(B9)}$$

On the other hand, using Eq. (11) results in

$$\boldsymbol{E}_p^{ind}(\boldsymbol{r}) = -\boldsymbol{p}_D \cdot (\nabla_{\boldsymbol{r}}\nabla_{\boldsymbol{r}'} g_{10}^{scat})_{\boldsymbol{r}'=\boldsymbol{r}_D} = \frac{1}{4\pi\epsilon_0}\frac{s^2-1}{\epsilon_b(s^2+2)}\frac{2p_D a^3}{r_D^3 r^3}(\hat{r}\, 2cos\theta + \hat{\theta}\, sin\theta). \quad \text{(B10)}$$

Comparing coefficients of Eq. (B9) and (B10) leads to

$$\alpha^p = \epsilon_b \frac{\epsilon_m/\epsilon_b - 1}{\epsilon_m/\epsilon_b + 2} a^3. \quad \text{(B11)}$$

Applying the same method for the quadrupole moment in Eq. B2,

$$\overleftrightarrow{Q}^{ind} = \frac{\alpha^Q p_D}{\epsilon_b r_D^4}\begin{pmatrix} -3 & 0 & 0 \\ 0 & -3 & 0 \\ 0 & 0 & 6 \end{pmatrix}. \quad \text{(B12)}$$

The electric field from an electric quadrupole can be obtained using[130]

$$\boldsymbol{E}_Q^{ind} = \frac{k_0^2}{\epsilon_0}\overleftrightarrow{G}^Q\left(\overleftrightarrow{Q}\boldsymbol{n}\right). \quad \text{(B13)}$$

Here, $\overleftrightarrow{G}^Q = \left[\frac{6i}{k^3r^3}\overleftrightarrow{I} - \frac{15i}{k^3r^3}\boldsymbol{n}\boldsymbol{n}^T\right]\frac{ik}{24\pi r}$ in the quasistatic limit, where $k = \frac{\omega}{c}\sqrt{\epsilon_b} = k_0\sqrt{\epsilon_b}$, and the superscript T means the transpose. Plugging in the quadrupole moment expression in Eq. (B13) results in

$$\boldsymbol{E}_Q^{ind} = -\frac{1}{4\pi\epsilon_0}\frac{9\alpha^Q p_D k_0^2}{2\epsilon_b k^2 r_D^4 r^4}\left(\hat{r}(1-3\cos^2\theta) + \hat{\theta}(-2\cos\theta\sin\theta)\right). \quad \text{(B14)}$$

On the other hand, using Eq. (11) results in

$$\boldsymbol{E}_Q^{ind} = -\frac{1}{\epsilon_0}\nabla_{\boldsymbol{r}}\left(\boldsymbol{p}_D \cdot (\nabla_{\boldsymbol{r}'} g_{20}^{scat})_{\boldsymbol{r}'=\boldsymbol{r}_D}\right)$$

$$= -\frac{1}{4\pi\epsilon_0}\frac{9p_D}{\epsilon_b r_D^4 r^4}\frac{2(\epsilon_m/\epsilon_b - 1)}{2\epsilon_m/\epsilon_b + 3}a^5\left(\hat{r}(1-3\cos^2\theta) + \hat{\theta}(-2\cos\theta\sin\theta)\right). \quad \text{(B15)}$$

Comparing the coefficients of Eq. (B14) and (B15) leads to

$$\alpha^Q = \epsilon_b\frac{\epsilon_m/\epsilon_b - 1}{\epsilon_m/\epsilon_b + \frac{3}{2}}a^5. \quad \text{(B16)}$$

As an aside, induced dipole and quadrupole polarizability for a plane wave source have been derived by solving Laplace's equation and using the boundary conditions at the surface of the sphere (Kelly et al.[1]), and comparing the far-zone scattered electric field expression from the induced multipole and the Mie theory (Evlyukhin et al.[126, 131]). It is also possible to use a similar approach as Evlyukhin et al.[126] in the near-zone, which is more suitable under the

quasistatic approximation (For derivation, see Chapter 5 of Bohren and Huffman[115] to obtain scattering coefficients in Mie theory in the quasistatic limit). The results are

$$\alpha^p = \epsilon_b \frac{\epsilon_m/\epsilon_b - 1}{\epsilon_m/\epsilon_b + 2} a^3 \quad \text{(B17)}$$

$$\alpha^Q = -\epsilon_b \frac{\epsilon_m/\epsilon_b - 1}{\epsilon_m/\epsilon_b + \frac{3}{2}} a^5. \quad \text{(B18)}$$

Finally, the quasistatic approximation may be lifted by adding correction factors. This is done by considering radiative damping and depolarization of the induced dipole,[1] [132] and as a result the factor

$$F^p_{Wokaun} = \frac{1}{1 - \frac{k^2}{a}\alpha^p - \frac{2}{3}ik^3\alpha^p} \quad \text{(B19)}$$

is multiplied by the quasistatic dipole polarizability $\alpha^p = \frac{1}{\epsilon_b}\frac{\epsilon_m/\epsilon_b - 1}{\epsilon_m/\epsilon_b + 2} a^3$ to obtain the modified dipole polarizability. This is sometimes called the modified long-wavelength approximation (MLWA). A more accurate correction factor can be achieved from Mie theory, by allowing more terms to survive in the scattering coefficient when applying the long wavelength approximation,[133] which results in

$$F^p_{Moroz} = \frac{1}{1 - \frac{3}{5}\left(1 - \frac{1}{\epsilon_m/\epsilon_b - 1}\right)\frac{k^2}{a}\alpha^p - \frac{2}{3}ik^3\alpha^p}, \quad \text{(B20)}$$

and a stricter approximation leads to[133]

$$F^p_{Mie} = \frac{1 - (\epsilon_m/\epsilon_b + 1)\frac{k^2 a^2}{10}}{1 - \frac{1}{10}(\epsilon_m/\epsilon_b + 10)\frac{k^2}{a}\alpha - \frac{2}{3}ik^3\alpha}. \quad \text{(B21)}$$

Following a similar procedure for the induced quadrupole leads to[134]

$$F^Q_{Mie} = \frac{1 - (\epsilon_m/\epsilon_b + 1)\frac{k^2 a^2}{14}}{1 - \frac{1}{14}\left(\epsilon_m/\epsilon_b + \frac{7}{2}\right)\frac{k^2}{a^3}\alpha^Q - \frac{1}{14}\left(1 + \frac{1}{8\epsilon_m/\epsilon_b - 1}\right)\frac{k^4}{a}\alpha^Q - \frac{1}{30}ik^5\alpha^Q} \quad \text{(B22)}$$

Applying these correction factors results in a red-shift of the resonance frequencies, and this effect grows with increasing particle size.

Appendix C. Analysis of Plasmon-Coupled Resonance Energy Transfer using Scalar Green's Function

In Section 5.5.2, it was pointed out that higher-order multipoles contribute more for larger particles and smaller dipole–particle separations in dipole–dipole PC-RET. This can be formally shown with the scalar Green's function for a sphere. It is readily seen from Eq. (B6) that the multipole contributions have a dependence on the size of the sphere (a) and the dipole–center of sphere distances ($r, r' > a$),

$$g_{lm}^{scat}(\boldsymbol{r}, \boldsymbol{r}'; \omega) \propto \frac{a^{2l+1}}{r'^{l+1} r^{l+1}}. \quad \text{(C1)}$$

For a donor dipole at $\boldsymbol{r}' = \boldsymbol{r}_D$ and an acceptor at $\boldsymbol{r} = \boldsymbol{r}_A$, using Eq. (11) shows that each multipolar contribution to the scattered electric field has the relation

$$\boldsymbol{E}_{lm}^{scat}(\boldsymbol{r}_A) \propto \frac{a^{2l+1}}{r_D^{l+2} r_A^{l+2}} = \frac{1}{a}\left(\frac{a}{r_D}\right)^{l+2}\left(\frac{a}{r_A}\right)^{l+2}. \quad \text{(C2)}$$

Thus, when $\frac{a}{r_D} \ll 1$ and $\frac{a}{r_A} \ll 1$, higher-order multipole contributions to the scattered field are small, and as $\frac{a}{r_D}$ and $\frac{a}{r_A}$ approach 1, higher-order modes become more important. Therefore, if the donor or the acceptor dipole is close enough to the sphere surface, it is necessary to consider higher order multipoles even for small particles in PC-RET and other processes involving the scattered electric field. A similar argument is possible for any source charge since $g(\boldsymbol{r}, \boldsymbol{r}'; \omega)$ is independent of the source.

Acknowledgement

This work was supported by NSF grant CHE-1760537. We thank Wendu Ding for valuable discussions.

References

[1] K. L. Kelly, E. Coronado, L. L. Zhao, G. C. Schatz: The Optical Properties of Metal Nanoparticles: The Influence of Size, Shape, and Dielectric Environment, The Journal of Physical Chemistry B **107**, 668-677 (2003)

[2] Y. Zhang, T. Nelson, S. Tretiak, H. Guo, G. C. Schatz: Plasmonic Hot-Carrier-Mediated Tunable Photochemical Reactions, ACS Nano **12**, 8415-8422 (2018)

[3] R. L. Gieseking, M. A. Ratner, G. C. Schatz: Review of Plasmon-Induced Hot-Electron Dynamics and Related Sers Chemical Effects. In: *Frontiers of Plasmon Enhanced Spectroscopy, Volume 1*, vol 1245, (American Chemical Society (ACS Symposium Series), 2016), pp. 1-22

[4] K. Ueno, H. Misawa: Surface Plasmon-Enhanced Photochemical Reactions, J. Photochem. Photobiol., C **15**, 31-52 (2013)

[5] S. Linic, U. Aslam, C. Boerigter, M. Morabito: Photochemical Transformations on Plasmonic Metal Nanoparticles, Nat. Mater. **14**, 567-576 (2015)

[6] S. Linic, P. Christopher, H. Xin, A. Marimuthu: Catalytic and Photocatalytic Transformations on Metal Nanoparticles with Targeted Geometric and Plasmonic Properties, Acc. Chem. Res. **46**, 1890-1899 (2013)

[7] S. Linic, P. Christopher, D. B. Ingram: Plasmonic-Metal Nanostructures for Efficient Conversion of Solar to Chemical Energy, Nat Mater **10**, 911-921 (2011)

[8] A. Lauchner, A. E. Schlather, A. Manjavacas, Y. Cui, M. J. McClain, G. J. Stec, F. J. Garcia de Abajo, P. Nordlander, N. J. Halas: Molecular Plasmonics, Nano Lett. **15**, 6208-6214 (2015)

[9] J. G. Smith, J. A. Faucheaux, P. K. Jain: Plasmon Resonances for Solar Energy Harvesting: A Mechanistic Outlook, Nano Today **10**, 67-80 (2015)

[10] M. L. Brongersma, N. J. Halas, P. Nordlander: Plasmon-Induced Hot Carrier Science and Technology, Nat. Nanotechnol. **10**, 25-34 (2015)

[11] T. G. U. Ghobadi, A. Ghobadi, E. Ozbay, F. Karadas: Strategies for Plasmonic Hot-Electron-Driven Photoelectrochemical Water Splitting, ChemPhotoChem **2**, 161-182 (2018)

[12] M. L. Brongersma, N. J. Halas, P. Nordlander: Plasmon-Induced Hot Carrier Science and Technology, Nature Nanotechnology **10**, 25 (2015)

[13] S. Linic, P. Christopher, D. B. Ingram: Plasmonic-Metal Nanostructures for Efficient Conversion of Solar to Chemical Energy, Nature Materials **10**, 911 (2011)

[14] K. Watanabe, D. Menzel, N. Nilius, H.-J. Freund: Photochemistry on Metal Nanoparticles, Chemical Reviews **106**, 4301-4320 (2006)
[15] J. Lee, S. Mubeen, X. Ji, G. D. Stucky, M. Moskovits: Plasmonic Photoanodes for Solar Water Splitting with Visible Light, Nano Lett. **12**, 5014-5019 (2012)
[16] S. Mukherjee, F. Libisch, N. Large, O. Neumann, L. V. Brown, J. Cheng, J. B. Lassiter, E. A. Carter, P. Nordlander, N. J. Halas: Hot Electrons Do the Impossible: Plasmon-Induced Dissociation of H2 on Au, Nano Lett. **13**, 240-247 (2013)
[17] S. Mukherjee, L. Zhou, A. M. Goodman, N. Large, C. Ayala-Orozco, Y. Zhang, P. Nordlander, N. J. Halas: Hot-Electron-Induced Dissociation of H2 on Gold Nanoparticles Supported on Sio2, Journal of the American Chemical Society **136**, 64-67 (2014)
[18] C. Zhang, H. Zhao, L. Zhou, A. E. Schlather, L. Dong, M. J. McClain, D. F. Swearer, P. Nordlander, N. J. Halas: Al–Pd Nanodisk Heterodimers as Antenna–Reactor Photocatalysts, Nano Letters **16**, 6677-6682 (2016)
[19] A. Marimuthu, J. Zhang, S. Linic: Tuning Selectivity in Propylene Epoxidation by Plasmon Mediated Photo-Switching of Cu Oxidation State, Science (Washington, DC, U. S.) **339**, 1590-1593 (2013)
[20] H. Robatjazi, H. Zhao, D. F. Swearer, N. J. Hogan, L. Zhou, A. Alabastri, M. J. McClain, P. Nordlander, N. J. Halas: Plasmon-Induced Selective Carbon Dioxide Conversion on Earth-Abundant Aluminum-Cuprous Oxide Antenna-Reactor Nanoparticles, Nat. Commun. **8**, 1-10 (2017)
[21] L. Zhou, D. F. Swearer, C. Zhang, H. Robatjazi, H. Zhao, L. Henderson, L. Dong, P. Christopher, E. A. Carter, P. Nordlander, N. J. Halas: Quantifying Hot Carrier and Thermal Contributions in Plasmonic Photocatalysis, Science (Washington, DC, U. S.) **362**, 69-72 (2018)
[22] M. Moskovits: The Case for Plasmon-Derived Hot Carrier Devices, Nat. Nanotechnol. **10**, 6-8 (2015)
[23] W.-r. Lee, S. Mubeen, G. D. Stucky, M. Moskovits: A Surface Plasmon Enabled Liquid-Junction Photovoltaic Cell, Faraday Discuss. **178**, 413-420 (2015)
[24] F. Wang, N. A. Melosh: Plasmonic Energy Collection through Hot Carrier Extraction, Nano Lett. **11**, 5426-5430 (2011)
[25] A. O. Govorov, H. Zhang, Y. K. Gun'ko: Theory of Photoinjection of Hot Plasmonic Carriers from Metal Nanostructures into Semiconductors and Surface Molecules, The Journal of Physical Chemistry C **117**, 16616-16631 (2013)
[26] U. Dasgupta, S. K. Saha, A. J. Pal: Plasmonic Effect in Pn-Junction Solar Cells Based on Layers of Semiconductor Nanocrystals: Where to Introduce Metal Nanoparticles?, Sol. Energy Mater. Sol. Cells **136**, 106-112 (2015)
[27] A. Naldoni, U. Guler, Z. Wang, M. Marelli, F. Malara, X. Meng, L. V. Besteiro, A. O. Govorov, A. V. Kildishev, A. Boltasseva, V. M. Shalaev: Broadband Hot-Electron Collection for Solar Water Splitting with Plasmonic Titanium Nitride, Advanced Optical Materials **5**, 1601031 (2017)
[28] H. Robatjazi, S. M. Bahauddin, C. Doiron, I. Thomann: Direct Plasmon-Driven Photoelectrocatalysis, Nano Letters **15**, 6155-6161 (2015)
[29] K. Wu, J. Chen, J. R. McBride, T. Lian: Efficient Hot-Electron Transfer by a Plasmon-Induced Interfacial Charge-Transfer Transition, Science **349**, 632 (2015)

[30] E. A. Sprague-Klein, M. O. McAnally, D. V. Zhdanov, A. B. Zrimsek, V. A. Apkarian, T. Seideman, G. C. Schatz, R. P. Van Duyne: Observation of Single Molecule Plasmon-Driven Electron Transfer in Isotopically Edited 4,4'-Bipyridine Gold Nanosphere Oligomers, J. Am. Chem. Soc. **139**, 15212-15221 (2017)

[31] E. A. Sprague-Klein, B. Negru, L. R. Madison, S. C. Coste, B. Rugg, A. M. Felts, M. O. McAnally, M. Banik, V. A. Apkarian, M. R. Wasielewshi, M. A. Ratner, T. Seideman, G. C. Schatz, R. P. Van Duyne: Photoinduced Plasmon-Driven Chemistry in Trans-1,2-Bis(4-Pyridyl)Ethylene Gold Nanosphere Oligomers J. Am. Chem. Soc. **140**, 10583-10592 (2018)

[32] H. Zhu, X. Ke, X. Yang, S. Sarina, H. Liu: Reduction of Nitroaromatic Compounds on Supported Gold Nanoparticles by Visible and Ultraviolet Light, Angewandte Chemie **122**, 9851-9855 (2010)

[33] S. Navalon, M. de Miguel, R. Martin, M. Alvaro, H. Garcia: Enhancement of the Catalytic Activity of Supported Gold Nanoparticles for the Fenton Reaction by Light, Journal of the American Chemical Society **133**, 2218-2226 (2011)

[34] X. Chen, H.-Y. Zhu, J.-C. Zhao, Z.-F. Zheng, X.-P. Gao: Visible-Light-Driven Oxidation of Organic Contaminants in Air with Gold Nanoparticle Catalysts on Oxide Supports, Angewandte Chemie International Edition **47**, 5353-5356 (2008)

[35] X. C. Huaiyong Zhu, Zhanfeng Zheng, Xuebin Ke, Esa Jaatinen, Jincai Zhao, Cheng Guo, Tengfeng Xie, Dejun Wang: Mechanism of Supported Gold Nanoparticles as Photocatalysts under Ultraviolet and Visible Light Irradiation, Chem. Comm, , 7524-7526 (2009)

[36] S. Mukherjee, F. Libisch, N. Large, O. Neumann, L. V. Brown, J. Cheng, J. B. Lassiter, E. A. Carter, P. Nordlander, N. J. Halas: Hot Electrons Do the Impossible: Plasmon-Induced Dissociation of H2 on Au, Nano Letters **13**, 240-247 (2013)

[37] P. Christopher, H. Xin, S. Linic: Visible-Light-Enhanced Catalytic Oxidation Reactions on Plasmonic Silver Nanostructures, Nature Chemistry **3**, 467 (2011)

[38] P. Christopher, H. Xin, A. Marimuthu, S. Linic: Singular Characteristics and Unique Chemical Bond Activation Mechanisms of Photocatalytic Reactions on Plasmonic Nanostructures, Nature Materials **11**, 1044 (2012)

[39] T. L. Thompson, J. T. Yates: Monitoring Hole Trapping in Photoexcited Tio2(110) Using a Surface Photoreaction, The Journal of Physical Chemistry B **109**, 18230-18236 (2005)

[40] J. T. Yates: Photochemistry on Tio2: Mechanisms Behind the Surface Chemistry, Surface Science **603**, 1605-1612 (2009)

[41] Z. Zhang, J. T. Yates: Direct Observation of Surface-Mediated Electron−Hole Pair Recombination in Tio2(110), The Journal of Physical Chemistry C **114**, 3098-3101 (2010)

[42] C. J. G. Cornu, A. J. Colussi, M. R. Hoffmann: Quantum Yields of the Photocatalytic Oxidation of Formate in Aqueous Tio2 Suspensions under Continuous and Periodic Illumination, The Journal of Physical Chemistry B **105**, 1351-1354 (2001)

[43] T. A. Westrich, K. A. Dahlberg, M. Kaviany, J. W. Schwank: High-Temperature Photocatalytic Ethylene Oxidation over Tio2, The Journal of Physical Chemistry C **115**, 16537-16543 (2011)

[44] A. A. Golubev, B. N. Khlebtsov, R. D. Rodriguez, Y. Chen, D. R. T. Zahn: Plasmonic Heating Plays a Dominant Role in the Plasmon-Induced Photocatalytic Reduction of 4-Nitrobenzenethiol, The Journal of Physical Chemistry C **122**, 5657-5663 (2018)
[45] T. Olsen, J. Gavnholt, J. Schiøtz: Hot-Electron-Mediated Desorption Rates Calculated from Excited-State Potential Energy Surfaces, Physical Review B **79**, 035403 (2009)
[46] X. Wu, E. S. Thrall, H. Liu, M. Steigerwald, L. Brus: Plasmon Induced Photovoltage and Charge Separation in Citrate-Stabilized Gold Nanoparticles, The Journal of Physical Chemistry C **114**, 12896-12899 (2010)
[47] E. S. Thrall, A. Preska Steinberg, X. Wu, L. E. Brus: The Role of Photon Energy and Semiconductor Substrate in the Plasmon-Mediated Photooxidation of Citrate by Silver Nanoparticles, The Journal of Physical Chemistry C **117**, 26238-26247 (2013)
[48] R. Jin, Y. Cao, C. A. Mirkin, K. L. Kelly, G. C. Schatz, J. G. Zheng: Photoinduced Conversion of Silver Nanospheres to Nanoprisms, Science **294**, 1901 (2001)
[49] R. Jin, Y. Charles Cao, E. Hao, G. S. Métraux, G. C. Schatz, C. A. Mirkin: Controlling Anisotropic Nanoparticle Growth through Plasmon Excitation, Nature **425**, 487 (2003)
[50] S. J. Lee, B. D. Piorek, C. D. Meinhart, M. Moskovits: Photoreduction at a Distance: Facile, Nonlocal Photoreduction of Ag Ions in Solution by Plasmon-Mediated Photoemitted Electrons, Nano Letters **10**, 1329-1334 (2010)
[51] A. Mills, S. Le Hunte: An Overview of Semiconductor Photocatalysis, Journal of Photochemistry and Photobiology A: Chemistry **108**, 1-35 (1997)
[52] A. Fujishima, K. Honda: Electrochemical Photolysis of Water at a Semiconductor Electrode, Nature **238**, 37 (1972)
[53] A. Fujishima, K. Honda: Kogyo Kagaku Zasshi **72**, 108 (1969)
[54] H. Kazuhito, I. Hiroshi, F. Akira: Tio 2 Photocatalysis: A Historical Overview and Future Prospects, Japanese Journal of Applied Physics **44**, 8269 (2005)
[55] A. Kudo, Y. Miseki: Heterogeneous Photocatalyst Materials for Water Splitting, Chemical Society Reviews **38**, 253-278 (2009)
[56] Y. Tian, T. Tatsuma: Mechanisms and Applications of Plasmon-Induced Charge Separation at Tio2 Films Loaded with Gold Nanoparticles, Journal of the American Chemical Society **127**, 7632-7637 (2005)
[57] C. Gomes Silva, R. Juárez, T. Marino, R. Molinari, H. García: Influence of Excitation Wavelength (Uv or Visible Light) on the Photocatalytic Activity of Titania Containing Gold Nanoparticles for the Generation of Hydrogen or Oxygen from Water, Journal of the American Chemical Society **133**, 595-602 (2011)
[58] K. Awazu, M. Fujimaki, C. Rockstuhl, J. Tominaga, H. Murakami, Y. Ohki, N. Yoshida, T. Watanabe: A Plasmonic Photocatalyst Consisting of Silver Nanoparticles Embedded in Titanium Dioxide, Journal of the American Chemical Society **130**, 1676-1680 (2008)
[59] P. Christopher, D. B. Ingram, S. Linic: Enhancing Photochemical Activity of Semiconductor Nanoparticles with Optically Active Ag Nanostructures: Photochemistry Mediated by Ag Surface Plasmons, The Journal of Physical Chemistry C **114**, 9173-9177 (2010)
[60] X. Zhou, C. Hu, X. Hu, T. Peng, J. Qu: Plasmon-Assisted Degradation of Toxic Pollutants with Ag−Agbr/Al2o3 under Visible-Light Irradiation, The Journal of Physical Chemistry C **114**, 2746-2750 (2010)

[61] E. A. Kowalska, Ryu; Ohtani, Bunsho: Visible Light-Induced Photocatalytic Reaction of Gold-Modified Titanium(Iv) Oxide Particles: Action Spectrum Analysis, Chem. Comm., 241-243 (2009)
[62] E. M. Kowalska, Orlando Omar Prieto; Abe, Ryu; Ohtani, Bunsho: Visible-Light-Induced Photocatalysis through Surface Plasmon Excitation of Gold on Titania Surfaces, Phys. Chem. Chem. Phys. **12**, 2344-2355 (2010)
[63] A. Primo, T. Marino, A. Corma, R. Molinari, H. García: Efficient Visible-Light Photocatalytic Water Splitting by Minute Amounts of Gold Supported on Nanoparticulate Ceo2 Obtained by a Biopolymer Templating Method, Journal of the American Chemical Society **133**, 6930-6933 (2011)
[64] Z. Liu, W. Hou, P. Pavaskar, M. Aykol, S. B. Cronin: Plasmon Resonant Enhancement of Photocatalytic Water Splitting under Visible Illumination, Nano Letters **11**, 1111-1116 (2011)
[65] E. Thimsen, F. Le Formal, M. Grätzel, S. C. Warren: Influence of Plasmonic Au Nanoparticles on the Photoactivity of Fe2o3 Electrodes for Water Splitting, Nano Letters **11**, 35-43 (2011)
[66] J.-J. Chen, J. C. S. Wu, P. C. Wu, D. P. Tsai: Plasmonic Photocatalyst for H2 Evolution in Photocatalytic Water Splitting, The Journal of Physical Chemistry C **115**, 210-216 (2011)
[67] D. B. Ingram, S. Linic: Water Splitting on Composite Plasmonic-Metal/Semiconductor Photoelectrodes: Evidence for Selective Plasmon-Induced Formation of Charge Carriers near the Semiconductor Surface, Journal of the American Chemical Society **133**, 5202-5205 (2011)
[68] Y. T. Tian, Tetsu: Plasmon-Induced Photoelectrochemistry at Metal Nanoparticles Supported on Nanoporous Tio2, Chem. Commun., 1810-1811 (2004)
[69] W. Zhai, S. Xue, A. Zhu, Y. Luo, Y. Tian: Plasmon-Driven Selective Oxidation of Aromatic Alcohols to Aldehydes in Water with Recyclable Pt/Tio2 Nanocomposites, ChemCatChem **3**, 127-130 (2010)
[70] A. C. Primo, Avelino; García Hermenegildo: Titania Supported Gold Nanoparticles as Photocatalyst, Phys. Chem. Chem. Phys. **13**, 886-910 (2011)
[71] M. K. Kumar, S. Krishnamoorthy, L. K. Tan, S. Y. Chiam, S. Tripathy, H. Gao: Field Effects in Plasmonic Photocatalyst by Precise Sio2 Thickness Control Using Atomic Layer Deposition, ACS Catalysis **1**, 300-308 (2011)
[72] S. K. Cushing, J. Li, F. Meng, T. R. Senty, S. Suri, M. Zhi, M. Li, A. D. Bristow, N. Wu: Photocatalytic Activity Enhanced by Plasmonic Resonant Energy Transfer from Metal to Semiconductor, Journal of the American Chemical Society **134**, 15033-15041 (2012)
[73] F. Libisch, J. Cheng, E. A. Carter: Electron-Transfer-Induced Dissociation of H2 on Gold Nanoparticles: Excited-State Potential Energy Surfaces Via Embedded Correlated Wavefunction Theory, Z. Phys. Chem. (Muenchen, Ger.) **227**, 1455-1466 (2013)
[74] F. Libisch, C. Huang, E. A. Carter: Embedded Correlated Wavefunction Schemes: Theory and Applications, Acc. Chem. Res. **47**, 2768-2775 (2014)
[75] R. L. Gieseking, M. A. Ratner, G. C. Schatz: Semiempirical Modeling of Ag Nanoclusters: New Parameters for Optical Property Studies Enable Determination of Double Excitation Contributions to Plasmonic Excitation, J. Phys. Chem. A **120**, 4542-4549 (2016)

[76] R. L. Gieseking, M. A. Ratner, G. C. Schatz: Quantum Mechanical Identification of Quadrupolar Plasmonic Excited States in Silver Nanorods, J. Phys. Chem. A **120**, 9324-9329 (2016)
[77] D. J. Trivedi, D. Wang, T. W. Odom, G. C. Schatz: Model for Describing Plasmonic Nanolasers Using Maxwell-Liouville Equations with Finite-Difference Time-Domain Calculations, Physical Review A **96**, 053825 (2017)
[78] J. G. Liu, H. Zhang, S. Link, P. Nordlander: Relaxation of Plasmon-Induced Hot Carriers, ACS Photonics **5**, 2584-2595 (2018)
[79] M. Bernardi, J. Mustafa, J. B. Neaton, S. G. Louie: Theory and Computation of Hot Carriers Generated by Surface Plasmon Polaritons in Noble Metals, Nature Communications **6**, 7044 (2015)
[80] J. Zhao, A. O. Pinchuk, J. M. McMahon, S. Li, L. K. Ausman, A. L. Atkinson, G. C. Schatz: Methods for Describing the Electromagnetic Properties of Silver and Gold Nanoparticles, Accounts of Chemical Research **41**, 1710-1720 (2008)
[81] H. Chen, J. M. McMahon, M. A. Ratner, G. C. Schatz: Classical Electrodynamics Coupled to Quantum Mechanics for Calculation of Molecular Optical Properties: A Rt-Tddft/Fdtd Approach, The Journal of Physical Chemistry C **114**, 14384-14392 (2010)
[82] J. Mullin, G. C. Schatz: Combined Linear Response Quantum Mechanics and Classical Electrodynamics (Qm/Ed) Method for the Calculation of Surface-Enhanced Raman Spectra, The Journal of Physical Chemistry A **116**, 1931-1938 (2012)
[83] J. Mullin, N. Valley, M. G. Blaber, G. C. Schatz: Combined Quantum Mechanics (Tddft) and Classical Electrodynamics (Mie Theory) Methods for Calculating Surface Enhanced Raman and Hyper-Raman Spectra, The Journal of Physical Chemistry A **116**, 9574-9581 (2012)
[84] J. L. Payton, S. M. Morton, J. E. Moore, L. Jensen: A Hybrid Atomistic Electrodynamics–Quantum Mechanical Approach for Simulating Surface-Enhanced Raman Scattering, Accounts of Chemical Research **47**, 88-99 (2014)
[85] J. M. Rinaldi, S. M. Morton, L. Jensen: A Discrete Interaction Model/Quantum Mechanical Method for Simulating Nonlinear Optical Properties of Molecules near Metal Surfaces, Molecular Physics **111**, 1322-1331 (2013)
[86] S. Bidault, A. Devilez, P. Ghenuche, B. Stout, N. Bonod, J. Wenger: Competition between Förster Resonance Energy Transfer and Donor Photodynamics in Plasmonic Dimer Nanoantennas, ACS Photonics **3**, 895-903 (2016)
[87] P. Ghenuche, J. de Torres, S. B. Moparthi, V. Grigoriev, J. Wenger: Nanophotonic Enhancement of the Förster Resonance Energy-Transfer Rate with Single Nanoapertures, Nano Letters **14**, 4707-4714 (2014)
[88] P. Ghenuche, M. Mivelle, J. de Torres, S. B. Moparthi, H. Rigneault, N. F. Van Hulst, M. F. García-Parajó, J. Wenger: Matching Nanoantenna Field Confinement to Fret Distances Enhances Förster Energy Transfer Rates, Nano Letters **15**, 6193-6201 (2015)
[89] X. Zhang, C. A. Marocico, M. Lunz, V. A. Gerard, Y. K. Gun'ko, V. Lesnyak, N. Gaponik, A. S. Susha, A. L. Rogach, A. L. Bradley: Experimental and Theoretical Investigation of the Distance Dependence of Localized Surface Plasmon Coupled Förster Resonance Energy Transfer, ACS Nano **8**, 1273-1283 (2014)

[90] X. Zhang, C. A. Marocico, M. Lunz, V. A. Gerard, Y. K. Gun'ko, V. Lesnyak, N. Gaponik, A. S. Susha, A. L. Rogach, A. L. Bradley: Wavelength, Concentration, and Distance Dependence of Nonradiative Energy Transfer to a Plane of Gold Nanoparticles, ACS Nano **6**, 9283-9290 (2012)
[91] L. Bujak, T. Ishii, D. K. Sharma, S. Hirata, M. Vacha: Selective Turn-on and Modulation of Resonant Energy Transfer in Single Plasmonic Hybrid Nanostructures, Nanoscale **9**, 1511-1519 (2017)
[92] L. Zhao, T. Ming, L. Shao, H. Chen, J. Wang: Plasmon-Controlled Förster Resonance Energy Transfer, The Journal of Physical Chemistry C **116**, 8287-8296 (2012)
[93] A. Dietrich, V. Buschmann, C. Müller, M. Sauer: Fluorescence Resonance Energy Transfer (Fret) and Competing Processes in Donor–Acceptor Substituted DNA Strands: A Comparative Study of Ensemble and Single-Molecule Data, Reviews in Molecular Biotechnology **82**, 211-231 (2002)
[94] L.-Y. Hsu, W. Ding, G. C. Schatz: Plasmon-Coupled Resonance Energy Transfer, The Journal of Physical Chemistry Letters **8**, 2357-2367 (2017)
[95] K. Nasiri Avanaki, W. Ding, G. C. Schatz: Resonance Energy Transfer in Arbitrary Media: Beyond the Point Dipole Approximation, J. Phys. Chem. C, doi:10.1021/acs.jpcc.8b07407Ahead of Print (2018)
[96] W. Ding, L.-Y. Hsu, G. C. Schatz: Plasmon-Coupled Resonance Energy Transfer: A Real-Time Electrodynamics Approach, The Journal of Chemical Physics **146**, 064109 (2017)
[97] W. Ding, L.-Y. Hsu, C. W. Heaps, G. C. Schatz: Plasmon-Coupled Resonance Energy Transfer Ii: Exploring the Peaks and Dips in the Electromagnetic Coupling Factor, The Journal of Physical Chemistry C **122**, 22650-22659 (2018)
[98] Y.-C. Yu, J.-M. Liu, C.-J. Jin, X.-H. Wang: Plasmon-Mediated Resonance Energy Transfer by Metallic Nanorods, Nanoscale Res Lett **8**, 209-209 (2013)
[99] Ł. Bujak, T. Ishii, D. K. Sharma, S. Hirata, M. Vacha: Selective Turn-on and Modulation of Resonant Energy Transfer in Single Plasmonic Hybrid Nanostructures, Nanoscale **9**, 1511-1519 (2017)
[100] V. N. Pustovit, A. M. Urbas, T. V. Shahbazyan: Energy Transfer in Plasmonic Systems, Journal of Optics **16**, 114015 (2014)
[101] K. Nasiri Avanaki, W. Ding, G. C. Schatz: Resonance Energy Transfer in Arbitrary Media: Beyond the Point Dipole Approximation, The Journal of Physical Chemistry C **122**, 29445-29456 (2018)
[102] A. O. Govorov, J. Lee, N. A. Kotov: Theory of Plasmon-Enhanced Förster Energy Transfer in Optically Excited Semiconductor and Metal Nanoparticles, Physical Review B **76**, 125308 (2007)
[103] X. M. Hua, J. I. Gersten, A. Nitzan: Theory of Energy Transfer between Molecules near Solid State Particles, The Journal of Chemical Physics **83**, 3650-3659 (1985)
[104] G. J. Daniels, R. D. Jenkins, D. S. Bradshaw, D. L. Andrews: Resonance Energy Transfer: The Unified Theory Revisited, The Journal of Chemical Physics **119**, 2264-2274 (2003)
[105] G. Juzeliūnas, D. L. Andrews: Quantum Electrodynamics of Resonant Energy Transfer in Condensed Matter, Physical Review B **49**, 8751-8763 (1994)
[106] D. Becerril, C. Noguez: Near-Field Energy Transfer between Nanoparticles Modulated by Coupled Multipolar Modes, Physical Review B **99**, 045418 (2019)

[107] M. Durach, A. Rusina, V. I. Klimov, M. I. Stockman: Nanoplasmonic Renormalization and Enhancement of Coulomb Interactions, New Journal of Physics **10**, 105011 (2008)
[108] N. V. Ilawe, M. B. Oviedo, B. M. Wong: Effect of Quantum Tunneling on the Efficiency of Excitation Energy Transfer in Plasmonic Nanoparticle Chain Waveguides, Journal of Materials Chemistry C **6**, 5857-5864 (2018)
[109] J.-S. Wu, Y.-C. Lin, Y.-L. Sheu, L.-Y. Hsu: Characteristic Distance of Resonance Energy Transfer Coupled with Surface Plasmon Polaritons, The Journal of Physical Chemistry Letters **9**, 7032-7039 (2018)
[110] L. Novotny, B. Hecht: *Principles of Nano-Optics*, (Cambridge University Press, New York 2006)
[111] H. T. Dung, L. Knöll, D.-G. Welsch: Intermolecular Energy Transfer in the Presence of Dispersing and Absorbing Media, Physical Review A **65**, 043813 (2002)
[112] S. H. Lin, L. J. Colangelo, H. Erying: Theoretical Analysis of Emission Spectra of Electronic Transitions of Molecules in Dense Media, Proceedings of the National Academy of Sciences **68**, 2135 (1971)
[113] S. H. Lin, G. Porter: On the Theory of Non-Radiative Transfer of Electronic Excitation, Proceedings of the Royal Society of London. A. Mathematical and Physical Sciences **335**, 51-66 (1973)
[114] D. P. Craig, T. Thirunamachandran: *Molecular Quantum Electrodynamics*, (Dover Publications, Mineola 1984)
[115] C. F. Bohren, D. R. Huffman: *Absorption and Scaterring of Light by Small Particles*, (John Wiley and Sons, 1983)
[116] T. Förster: Zwischenmolekulare Energiewanderung Und Fluoreszenz, Annalen der Physik **437**, 55-75 (1948)
[117] H.-J. Son, S. Jin, S. Patwardhan, S. J. Wezenberg, N. C. Jeong, M. So, C. E. Wilmer, A. A. Sarjeant, G. C. Schatz, R. Q. Snurr, O. K. Farha, G. P. Wiederrecht, J. T. Hupp: Light-Harvesting and Ultrafast Energy Migration in Porphyrin-Based Metal–Organic Frameworks, Journal of the American Chemical Society **135**, 862-869 (2013)
[118] K. Shankar, X. Feng, C. A. Grimes: Enhanced Harvesting of Red Photons in Nanowire Solar Cells: Evidence of Resonance Energy Transfer, ACS Nano **3**, 788-794 (2009)
[119] B. E. Hardin, E. T. Hoke, P. B. Armstrong, J.-H. Yum, P. Comte, T. Torres, J. M. J. Fréchet, M. K. Nazeeruddin, M. Grätzel, M. D. McGehee: Increased Light Harvesting in Dye-Sensitized Solar Cells with Energy Relay Dyes, Nature Photonics **3**, 406 (2009)
[120] J. Li, S. K. Cushing, F. Meng, T. R. Senty, A. D. Bristow, N. Wu: Plasmon-Induced Resonance Energy Transfer for Solar Energy Conversion, Nature Photonics **9**, 601 (2015)
[121] Y. Choi, T. Kang, L. P. Lee: Plasmon Resonance Energy Transfer (Pret)-Based Molecular Imaging of Cytochrome C in Living Cells, Nano Letters **9**, 85-90 (2009)
[122] Y. Choi, Y. Park, T. Kang, L. P. Lee: Selective and Sensitive Detection of Metal Ions by Plasmonic Resonance Energy Transfer-Based Nanospectroscopy, Nature Nanotechnology **4**, 742 (2009)
[123] J. Ling, C. Z. Huang: Energy Transfer with Gold Nanoparticles for Analytical Applications in the Fields of Biochemical and Pharmaceutical Sciences, Analytical Methods **2**, 1439-1447 (2010)

[124] D. Martín-Cano, L. Martín-Moreno, F. J. García-Vidal, E. Moreno: Resonance Energy Transfer and Superradiance Mediated by Plasmonic Nanowaveguides, Nano Letters **10**, 3129-3134 (2010)
[125] J. de Torres, P. Ferrand, G. Colas des Francs, J. Wenger: Coupling Emitters and Silver Nanowires to Achieve Long-Range Plasmon-Mediated Fluorescence Energy Transfer, ACS Nano **10**, 3968-3976 (2016)
[126] A. B. Evlyukhin, C. Reinhardt, U. Zywietz, B. N. Chichkov: Collective Resonances in Metal Nanoparticle Arrays with Dipole-Quadrupole Interactions, Physical Review B **85**, 245411 (2012)
[127] M. Kerker, D. S. Wang, H. Chew: Surface Enhanced Raman Scattering (Sers) by Molecules Adsorbed at Spherical Particles, Appl. Opt. **19**, 3373-3388 (1980)
[128] L. L. D. Julian Schwinger, Jr., Kimball A. Milton, Wu-yang Tsai: *Classical Electrodynamics*, (Perseus Books, Reading 1998)
[129] C. Cherqui: The Effect of Dynamical Image Forces on the Transport Properties of Charge Carriers and Excitons in Metal-Semiconductor Nanostructures, Ph.D. Thesis (Department of Physics and Astronomy, University of New Mexico, 2014)
[130] A. B. Evlyukhin, C. Reinhardt, B. N. Chichkov: Multipole Light Scattering by Nonspherical Nanoparticles in the Discrete Dipole Approximation, Physical Review B **84**, 235429 (2011)
[131] A. B. Evlyukhin, C. Reinhardt, A. Seidel, B. S. Luk'yanchuk, B. N. Chichkov: Optical Response Features of Si-Nanoparticle Arrays, Physical Review B **82**, 045404 (2010)
[132] M. Meier, A. Wokaun: Enhanced Fields on Large Metal Particles: Dynamic Depolarization, Opt. Lett. **8**, 581-583 (1983)
[133] A. Moroz: Depolarization Field of Spheroidal Particles, J. Opt. Soc. Am. B **26**, 517-527 (2009)
[134] W. Ding: Massachusetts Institute of Technology, Personnal communication, (2018)